

New Routes for Multicomponent Atomically Precise Metal Nanoclusters

Esma Khatun and Thalappil Pradeep*



Cite This: *ACS Omega* 2021, 6, 1–16



Read Online

ACCESS |

 Metrics & More

 Article Recommendations

ABSTRACT: Atomically precise metal nanoclusters (NCs), protected by a monolayer of ligands, are regarded as potential building blocks for advanced technologies. They are considered as intermediates between the atomic/molecular regime and the bulk. Incorporation of foreign metals in NCs enhances several of their properties such as catalytic activity, luminescence, and so on; hence, it is of high importance for tuning their properties and broadening the scope of applications. In most of the cases, enhancement in specific properties was observed upon alloying due to the synergistic effect. In the past several years, many alloy clusters have been synthesized, which show a tremendous change in the properties than their monometallic analogs. However, controlling the synthesis and tuning the structures of alloy NCs with atomic precision are major challenges. Various synthetic methodologies have been developed so far for the controlled synthesis of alloy NCs. In this perspective, we have highlighted those diverse synthetic routes to prepare alloys, which include co-reduction, galvanic reduction, antialgalvanic reduction, metal deposition, ligand exchange, intercluster reaction, and reaction of NCs with bulk metals. Advancement in synthetic procedures will help in the preparation of alloy NCs with the desired structure and composition. Future perceptions concerning the progress of alloy nanocluster science are also provided.



1. INTRODUCTION

There is a rich and fascinating history for metals and their alloys.^{1–3} Alloys have been known from ancient times; bronze (90% Cu and 10% Sn) was the first to be invented circa BC 3500. Nanoscience has provided a new direction to the subject of metals and their alloys.^{4–6} The famous Lycurgus cup known since the 4th century AD is one of the earliest known applications of nanotechnology.⁷ It is found to be composed of nanoparticles of Ag, Au, and Cu of 50–100 nm in size, dispersed in a glass matrix.⁸ The cup changes its color in different light, greenish in reflected light, and reddish in transmitted light. The nanoalloy particles of different sizes in the cup are responsible for this color change. Michael Faraday observed the unusual behavior of finely divided metal particles in their colloids in 1857.⁹ Their optical properties are now known to be due to surface plasmon excitations. Nanoparticles with monolayer protection were prepared over a century later, enabling the synthesis of solid powders of such freely dispersible particles. They also show similar optical characteristics. Nanoclusters (NCs), which are atomically precised, are the smallest analogues of such ligand-protected nanoparticles and they exhibit unique optical, electronic, dielectric, magnetic, and chemical properties.^{10,11} These properties are strongly dependent on the composition and geometric variations. The combination of two or more metals in NCs modify several of their properties, often leading to enhancement in the desired properties such as luminescence, catalysis, etc.^{12–14} Therefore,

the main objective of multicomponent alloy NC science is to explore the rich variety of alloys and their interesting properties.

The synthesis of solution-phase Au NCs protected by phosphine ligands was started in 1969–1970 and a few phosphine-protected bi- and trimetallic NCs were also prepared.^{15–19} After a long gap, in 2005, Shichibu *et al.* synthesized Au₂₅(SG)₁₈ (SG = glutathione) by ligand exchange from phosphine-protected Au NCs.²⁰ Glutathione was used for the synthesis of gold nanoparticles by Whetten *et al.*²¹ After that, many NCs have been prepared with ligand protection. More than 300 monometallic NCs of Au, Ag, and Cu have been synthesized by various synthetic methods. However, the number of multimetallic NCs is less.^{22–33} Among them, the number of bimetallic NCs is higher than trimetallic and tetrametallic ones.^{34–42}

During the synthesis of alloy NCs, mixtures of products get formed. For unambiguous characterization of the formed NC, it is important to purify or separate the as-synthesized NCs. Several separation techniques such as gel electrophoresis⁴³ and

Received: October 2, 2020

Accepted: December 8, 2020

Published: December 18, 2020

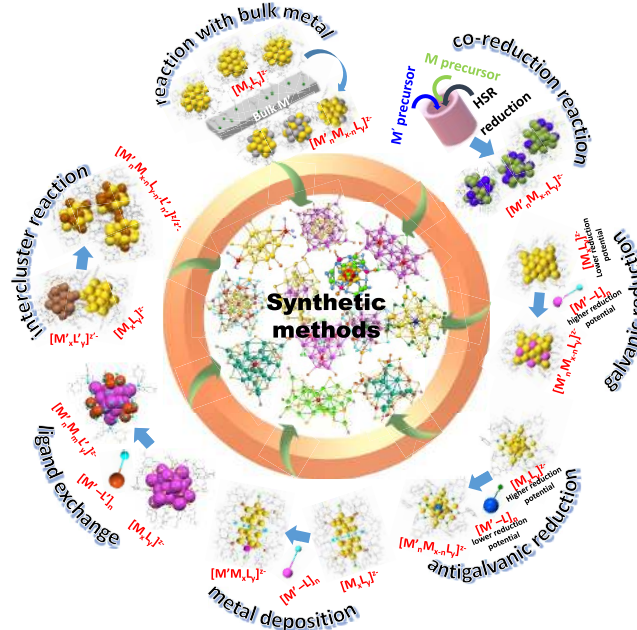


size exclusion chromatography (SEC)⁴⁴ have made tremendous contributions to the science of metal NCs and their alloys. In 2005, Tsukuda *et al.* separated the mixture of glutathione-protected Au NCs such as Au₁₀(SG)₁₀, Au₁₅(SG)₁₃, Au₁₈(SG)₁₄, Au₂₂(SG)₁₆, Au₂₂(SG)₁₇, Au₂₅(SG)₁₈, Au₂₉(SG)₂₀, Au₃₃(SG)₂₂, and Au₃₉(SG)₂₄ using polyacrylamide gel electrophoresis (PAGE).⁴⁵ Other than SEC, high-performance liquid chromatography (HPLC) and thin-layer chromatography (TLC) are used widely for purification and separation of clusters. The composition of alloy NCs can be probed by high-resolution electrospray ionization (ESI) and matrix-assisted laser desorption ionization (MALDI) mass spectrometry (MS).^{42,46} In 2005, compositions of a series of glutathione-protected Au NCs separated by PAGE technique were determined mass-spectrometrically. Later, Whetten *et al.* unambiguously assigned the composition of the most popular NC in this family, Au₂₅(PET)₁₈ (PET = 2-phenylethanethiol), through ESI MS in 2007.⁴⁷ Although the composition of alloy NCs can be examined by MS, the exact structure and position of dopants can be understood only by using single-crystal X-ray diffraction (SCXRD). The structure of Au₂₅(PET)₁₈ was solved in 2008 and, in 2014, the first X-ray crystal structure of Ag_xAu_{25-x}(PET)₁₈ was determined.^{22,47,48} Recently, electron diffraction has been used to resolve the structures of those NCs for which crystallization is difficult.⁴⁹ In addition to the experimental methods, computation has also contributed significantly for understanding the structures and properties of these clusters.^{22,50–53}

To understand the origin of optical and electronic properties of NCs, the substitution of metal atoms by another element is worthwhile. For example, the emission intensity of rod-like [Au₂₅(PPh₃)₁₀(SR)₅Cl₂]²⁺ can be enhanced 200-fold by substituting 13 Au atoms with Ag.⁵⁴ The doped NC, [Ag₁₃Au₁₂(PPh₃)₁₀(SR)₅Cl₂]²⁺, having the same structure and nuclearity exhibits 40% photoluminescence quantum yield. An interesting change in the UV–vis spectrum of Au₂₅(SR)₁₈ was seen after single Pd/Pt doping.^{55–57} The change in electronic structure upon doping with Pd/Pt led to the enhancement of catalytic efficiency toward hydrogen evolution reaction than with the undoped parent cluster, Au₂₅(SR)₁₈. The stability of the NC was enhanced due to doping. Unlike Pd/Pt, multiple Au atoms were replaced by Ag atoms and, depending on the number of doped Ag atoms, the electronic and catalytic properties differ.^{58,59} The silver analogue of Au₂₅(SR)₁₈, namely, Ag₂₅(SR)₁₈, also showed different optical and electronic properties upon doping with Pd, Pt, and Au atoms.^{60,61} The yellow color of Ag₂₅(SR)₁₈ turned to greenish-yellow while being doped with Pd and the color turned dark green upon doping with Pt and Au. Also, the singly doped Ag₂₅(SR)₁₈ with Pd, Pt, and Au exhibited higher catalytic performance.⁶² Doping can induce chirality in NCs. For example, the incorporation of three Ag atoms in Au₁₈(2,4-DMBT)₁₄ (DMBT = dimethylbenzenethiol) transformed the achiral NC into the chiral system.^{63,64} Also, the doping of Ag in Au₃₈(SR)₂₄ induced chirality. Along with a significant change in circular dichroism (CD) spectrum, Ag_xAu_{38-x}(SR)₂₄ lowers the racemization temperature.³⁶ The doped foreign atoms prefer to occupy certain positions in the parent NC. Pd, Ni, Pt, and Cd atoms always prefer to occupy the center, whereas Ag and Au atoms can be doped in all the possible positions. But Cu atoms always prefer outer staple positions.⁶⁵ Hence, by proper combinations, more than one metal atom can be incorporated to make multicomponent alloy NCs.

In this perspective article, we focus on the various synthetic methods used for making multimetallic alloy NCs (Scheme 1).

Scheme 1. Schematic Representation of Various Synthetic Methodologies of Alloy NCs^a



^aCo-reduction, galvanic reduction, antigalvanic reduction, metal deposition, ligand exchange, intercluster reaction, and reaction of NCs with bulk metal are illustrated.

At first, we discuss the classical methods used for the preparation of alloy NCs such as co-reduction and galvanic and antigalvanic reduction methods. After that, we discuss the other emerging procedures for the formation of alloy NCs, which are metal deposition, ligand exchange, intercluster reactions, and reaction between NCs and bulk metals. In the case of co-reduction method, the structure and composition cannot be controlled, while galvanic and antigalvanic exchange reaction methods are used for making a large number of alloy NCs, keeping the structural integrity the same as that of the monometallic analogues. Metal deposition certainly changes the composition; however, the total structure of the parent cluster remains unaltered. Ligand exchange method, which is a well-established method for the preparation of noble metal NCs, is now being used for the synthesis of alloy NCs with new atomicity and properties. Other than galvanic and antigalvanic reduction methods, a new synthetic method has been discussed in detail where reaction involving two different NCs (named as intercluster reaction) leads to the formation of structure-conserved alloy NCs. Such intercluster reactions between Ag and Au NCs are illustrated here. Similar to the reaction between two NCs, NC was found to react with bulk metals also. For more detailed information about the structures and properties of NCs, we direct the readers to several recent review articles.^{13,61,66–70}

2. CO-REDUCTION METHOD

Co-reduction is a kind of Brust–Schiffrin method where, instead of one metal precursor, several metal precursors are mixed with appropriate protective ligands and the reduction is performed with suitable reducing agents. The method is also known as the direct reduction method. With the help of this synthetic

Table 1. List of Alloy NCs, Their Method of Synthesis, and Characterization Methods Used

no	core	ligand	alloy cluster	focus	method of synthesis	reference
1	Au ₂ Cd	phenylethylthiol	Au ₂ Cd(PET) ₁₈	crystal structure	antigalvanic exchange	91,92
2	Au ₂ Hg	phenylethylthiol	Au ₂ Hg(PET) ₁₈	mass spectrometry	antigalvanic exchange	91,92
3	Au ₁₅ Ag ₃	2,4-dimethylbenzenethiol	Au ₁₅ Ag ₃ (2,4-DMBT) ₁₄	crystal structure	antigalvanic exchange	63
4	Au ₉ M ₄ (M = Ag, Cu)	diphenylmethylphosphine	[Au ₉ M ₄ Cl ₄ (PMePh ₂) ₈][C ₂ B ₉ H ₁₂] ⁻ ·CH ₂ Cl ₂ (M = Ag, Cu)	FAB mass spectrometry	antigalvanic exchange	93
5	Au _{3-x} Cu _x	cyclohexanethiol	[Au _{3-x} Cu _x (CHT) ₁₆] ⁻	crystal structure	antigalvanic exchange	94
6	M ₁ Ag _x Au _{24-x} (M = Cd/Hg)	phenylethanethiol	M ₁ Ag _x Au _{24-x} (PET) ₁₈ (M = Cd/Hg)	mass spectrometry	antigalvanic exchange	41
7	AgAu ₁₇	hexanethiol	AgAu ₁₇ (HT) ₁₄	crystal structure	antigalvanic exchange	95
8	Au _{24-x-y} Ag _x Cu _y Pd	1-dodecanethiol	Au _{24-x-y} Ag _x Cu _y Pd(SC ₁₂ H ₂₅) ₁₈	mass spectrometry	antigalvanic exchange	96
9	Au ₃₈ Cu ₁	2-phenylethanethiol	Au ₃₈ Cu ₁ (2-PET) ₂₄	mass spectrometry	antigalvanic exchange	97
10	(Ag-Au) ₁₄₄	phenylethanethiol	(Ag-Au) ₁₄₄ (PET) ₆₀	mass spectrometry	co-reduction	83
11	Au _{144-x} Cu _x	hexanethiol	Au _{144-x} Cu _x (HT) ₆₀	mass spectrometry	co-reduction	82
12	Ag ₄ Ni ₂	dimercaptosuccinic acid	Ag ₄ Ni ₂ (DMSA) ₄	mass spectrometry	co-reduction	80
13	Ag ₄ Pt ₂	dimercaptosuccinic acid	Ag ₄ Pt ₂ (DMSA) ₄	mass spectrometry	co-reduction	98
14	Ag ₄ Pd ₂	dimercaptosuccinic acid	Ag ₄ Pd ₂ (DMSA) ₄	crystal structure	co-reduction	99
15	Au ₁₃ Cu _x (x = 2, 4, 8)	pyridine-2-thiol, triphenylpyridine 4- <i>tert</i> -butylbenzenethiol pyridinediphenylphosphine	Au ₁₃ Cu _x (PPH ₃) ₆ (SPy) ₆ ⁺ Au ₁₃ Cu ₄ (PPH ₃ Py) ₄ (SC ₆ H ₄ - <i>tert</i> -C ₄ H ₉) ₈ ⁺ Au ₁₃ Cu ₈ (PPH ₃ Py) ₁₂ ⁺	crystal structures	co-reduction	100
16	Ag ₂₈ Cu ₁₂	2,4-dichlorobenzenethiol	[Ag ₂₈ Cu ₁₂ (2,4-DCBT) ₂₄] ⁻⁴	crystal structure	co-reduction	85
17	Au ₂₄ Ag ₂₀	phenylalkynyl, 2-pyridylthiolate	Au ₂₄ Ag ₂₀ (2-Spy) ₄ (PhC≡C) ₂₀ Cl ₂	crystal structure	co-reduction	101
18	Ag ₂₄ Pd	2,4-dichlorobenzenethiol	(PPH ₃) ₂ [Ag ₂₄ Pd(2,4-DCBT) ₁₈]	crystal structure	co-reduction	60
19	Ag ₂₄ Pt	2,4-dichlorobenzenethiol	(PPH ₃) ₂ [Ag ₂₄ Pt(2,4-DC) ₁₈] (x = 1, 2)	crystal structure	co-reduction	60
20	Ag ₂₄ Ni	2,4-dimethylbenzenethiol	(PPH ₃) ₂ [Ag ₂₄ Ni(SR) ₁₈]	mass spectrometry	co-reduction	89
21	Au ₈₀ Ag ₃₀	phenylalkene	[Au ₈₀ Ag ₃₀ (PhC≡C) ₄₂ Cl ₉] ⁻¹	crystal structure	co-reduction	84
22	Au ₂₄ Pd	phenylethanethiol	[Au ₂₄ Pd(PET) ₁₈] ⁻¹	crystal structure	co-reduction	57,102
23	Au ₂₄ Pt	phenylethanethiol	[Au ₂₄ Pt(PET) ₁₈]	crystal structure	co-reduction	55,102
24	Au ₃₇ Pd ₁	phenylethanethiol	Au ₃₇ Pd ₁ (PET) ₂₄	mass spectrometry	co-reduction	56
25	Au ₃₆ Pd ₂	phenylethanethiol	Au ₃₆ Pd ₂ (PET) ₂₄	mass spectrometry	co-reduction	56,103
26	Ag ₂ Au _{38-x}	phenylethanethiol	Ag ₂ Au _{38-x} (PET) ₂₄	crystal structure	co-reduction	36
27	Ag ₆ Au ₂₄	<i>tert</i> -butyl hydroperoxide	[Ag ₆ Au ₂₄ (TBHP) ₃₂] ²⁺	crystal structure	co-reduction	86
28	Au ₁₂ Ag ₁₂ Ni	hexafluoroantimonate, triphenylphosphine	[Au ₁₂ Ag ₁₂ Ni(PPH ₃) ₁₀ Cl ₇][SbF ₆]	crystal structure	co-reduction	18
29	Au ₁₂ Ag ₁₂ Pt	triphenylphosphine	[Au ₁₂ Ag ₁₂ Pt(PPH ₃) ₁₀ Cl ₇] ⁻¹	crystal structure	co-reduction	18
30	Ag ₃ Au ₁₂	diphenylmethylphosphine	(MePh ₂ P) ₁₀ Au ₁₂ Ag ₃ Br ₉	crystal structure	co-reduction	104
31	Au ₁₈ Ag ₂₀	<i>para</i> -tolylphosphine	[(<i>p</i> -Tol ₃ P) ₁₂ Au ₁₈ Ag ₂₀ Cl ₁₄]	crystal structure	co-reduction	7
32	Au ₂₄ Ag ₂₄	triphenylphosphine	[(Ph ₃ P) ₁₂ Au ₂₄ Ag ₂₄ Cl ₁₀]	crystal structure	co-reduction	74
33	AuAg ₁₉	<i>O,O</i> -diisopropyl dithiophosphate	[AuAg ₁₉ (S ₂ P(O ⁱ Pr) ₂) ₁₂]	crystal structure	co-reduction	105
34	AuAg ₂₄	1,1-bis(diphenylphosphino)methane, cyclohexanethiol	[AuAg ₂₄ (Dppm) ₃ (CHT) ₁₇] ²⁺	crystal structure	co-reduction	106
35	Pt ₂ Ag ₃	triphenylphosphine	[Pt ₂ Ag ₃ Cl ₇ (PPH ₃) ₁₀]	crystal structure	co-reduction	107
36	AuAg ₁₆	<i>tert</i> -butylbenzenethiol	(TOA) ₂ AuAg ₁₆ (TBTT) ₁₂	crystal structure	co-reduction	87
37	Ag ₂₆ Pt	2-ethylbenzenethiol	Ag ₂₆ Pt(2-EBT) ₁₈ (PPH ₃) ₆	crystal structure	co-reduction	108
38	Au ₂ Cu ₆	adamentanethiol, diphenylpyridinephosphine	Au ₂ Cu ₆ (S-Adm) ₆ (PPH ₂ Py) ₂	crystal structure	co-reduction	109
39	Au ₄ Ag ₅	adamentanethiol, 1,1-bis(diphenylphosphino)methane	[Au ₄ Ag ₅ (dppm) ₂ (SAdm) ₆] ⁺	crystal structure	co-reduction	110
40	Au ₄ Ag ₂₃	1,1'-bis(diphenylphosphino)ferrocene, <i>tert</i> -butylalkynyl	[Au ₄ Ag ₂₃ (C≡CBut) ₁₀ Cl ₇ (dppf) ₄] ²⁺	crystal structure	co-reduction	39

Table 1. continued

no	core	ligand	alloy cluster	focus	method of synthesis	reference
41	Au ₅ Ag ₂₄	1,1'-bis(diphenylphosphino)ferrocene, <i>tert</i> -butylbenzylthiol	[Au ₅ Ag ₂₄ (C≡CC ₆ H ₄ P-But) ₁₆ (dppf) ₄ Cl ₄] ³⁺	crystal structure	co-reduction	39
42	Au _x Ag _{59-x}	1,3-benzenedithiol, triphenylphosphine	Au _x Ag _{59-x} (BDT) ₁₂ (PPh ₃) ₄	crystal structure, mass spectrometry	co-reduction	35
43	Au _{33-x} Ag _x	cyclohexanethiol	Au _{33-x} Ag _x (S-Adm) ₁₆	crystal structure	co-reduction	111
44	Au ₁₉ Cd ₂	cyclohexanethiol	[Au ₁₉ Cd ₂ (CHT) ₁₆] ⁻	crystal structure	co-reduction	94
45	Cu ₃₀ Ag ₆₁	adamentanethiol, tetraphenylborate	[Cu ₃₀ Ag ₆₁ (SAdm) ₃₈ S ₃](BPh ₄)	crystal structure	co-reduction	112
46	Au ₄ Cu ₄	adamentanethiol, 1,1-bis(diphenylphosphino)methane	[Au ₄ Cu ₄ (Dppm) ₂ (SAdm) ₃] ⁺ Br	crystal structure	co-reduction	113
47	Au ₈ Ag ₅₇	1,3-bis(diphenylphosphino)propane, cyclohexanethiol	[Au ₈ Ag ₅₇ (Dppp) ₄ (CHT) ₃ Cl ₂] ⁺ Cl	crystal structure	co-reduction	114
48	Pt ₁ Ag ₉	tris(4-fluorophenyl)phosphine	Pt ₁ Ag ₉ [P(Ph-F) ₃] ₃ Cl ₃	crystal structure	co-reduction	115
49	Au _{130-x} Ag _x	<i>tert</i> -butylbenzenethiol	Au _{130-x} Ag _x (TBBT) ₅₅	crystal structure	co-reduction	116
50	Ag ₁₇ Cu ₁₂	1,3-benzenedithiol, triphenylphosphine	Ag ₁₇ Cu ₁₂ (BDT) ₁₂ (PPh ₃) ₄	crystal structure	co-reduction	117
51	Au ₇ Ag ₉	1,1'-bis(diphenylphosphino)ferrocene	[Au ₇ Ag ₉ (dppf) ₃ (CF ₃ CO ₂) ₂ BF ₄] _n	crystal structure	co-reduction	118
52	Ag ₂₀ Cu ₁₂	2,4-dimethylbenzenethiol, 1,1-bis(diphenylphosphino)methane	[Ag ₂₀ Cu ₁₂ (2,4-DMBT) ₁₄ (Dppm) ₆ Br ₈] ²⁺	crystal structure	co-reduction	119
53	Au ₉ Ag ₁₂	1-adamantanethiol/ <i>tert</i> -butylmercaptan, 1,1-bis(diphenylphosphino)methane	[Au ₉ Ag ₁₂ (SR) ₄ (dppm) ₆ X ₆] ³⁺	crystal structure	co-reduction	120
54	PtAu ₈	triphenylphosphine	PtAu ₈ (PPh ₃) ₈ (NO ₃) ₂	crystal structure	co-reduction	121
55	Au _{12-n} Cu ₃₂	4-(trifluoromethyl)thiophenol	Au _{12-n} Cu ₃₂ (SR) _{30-n}] ⁴⁻ (n = 0, 2, 4, 6)	crystal structure	co-reduction	122
56	Cd ₁ Au ₁₄	<i>tert</i> -butylthiol	Cd ₁ Au ₁₄ (S ^t Bu) ₁₂	crystal structure	co-reduction	123
57	Au ₈ Ag ₃	triphenylphosphine	Au ₈ Ag ₃ (PPh ₃) ₃ Cl ₃	crystal structure	co-reduction	124
58	Au _{36-x} Ag _x	<i>tert</i> -butylbenzenethiol	Au _{36-x} Ag _x (SPh- ^t Bu) ₂₄	mass spectrometry	co-reduction	125
59	Au _{38-x} Cu _x	2,4-dimethylbenzenethiol	Au _{38-x} Cu _x (2,4-DMBT) ₂₄ (x = 0–6)	crystal structure	co-reduction	126
60	Au ₁₉ Cu ₃₀	3-ethynylthiophene/ethynylbenzene	[Au ₁₉ Cu ₃₀ (C≡C) ₂₂ (Ph ₃ P) ₆ Cl ₂]	crystal structure	co-reduction	127
61	Au ₃ Ag ₃₈	phenylethanethiol	[Au ₃ Ag ₃₈ (PET) ₂₄ X ₅] ²⁻ (X = Cl or Br)	crystal structure	co-reduction	128
62	Au ₄ Pt ₂	phenylethanethiol	Au ₄ Pt ₂ (PET) ₈	crystal structure	co-reduction	129
63	Au ₄ Pd ₂	phenylethanethiol	Au ₄ Pd ₂ (PET) ₈	crystal structure	co-reduction	130
64	Au ₂ Cu ₆	<i>tert</i> -butyl benzenethiol	Au ₂ Cu ₆ (TBBT) ₂₂	crystal structure	co-reduction	131
65	Au _{36-x} Cu _x	<i>m</i> -methylbenzenethiol	Au _{36-x} Cu _x (<i>m</i> -MBT) ₂₄ (x = 1–3)	crystal structure	co-reduction	132
66	Au ₁₃ Cu ₂	1,3-bis(diphenylphosphino)propane, pyridine-2-thiol, (2 <i>r</i> ,4 <i>r</i>)/(2 <i>s</i> ,4 <i>s</i>)-2,4-bis(diphenylphosphino)pentane	Au ₁₃ Cu ₂ (DPPP) ₃ (SPY) ₆ , Au ₁₃ Cu ₂ ((2 <i>r</i> ,4 <i>r</i>)/(2 <i>s</i> ,4 <i>s</i>)-BDPP) ₃ (SPY) ₆	crystal structure	co-reduction	81
67	PtAu ₇	triphenylphosphine	[Pt(H)(PPh ₃)(AuPPh ₃) ₇] ²⁺	crystal structure	co-reduction	90
68	Ag ₃₂ Au ₁₂	fluorobenzenethiol	Ag ₃₂ Au ₁₂ (FTP) ₃₀] ¹⁴⁻	crystal structure	co-reduction, intercluster reaction	31,133
69	Au _{21-x} Ag _x	<i>tert</i> -butylthiol	Au _{21-x} Ag _x (TBT) ₁₅ (x = 4–8)	crystal structure	co-reduction, ligand exchange	134
70	Au _{21-x} Cu _x	<i>tert</i> -butylthiol	Au _{21-x} Cu _x (TBT) ₁₅ (x = 0, 1), Au _{21-x} Cu _x (TBT) ₁₅ (x = 2–5)	crystal structure	co-reduction, ligand exchange	134
71	Au _{25-x} Ag _x (x = 6–8)	phenylethanethiol	[Au _{25-x} Ag _x (PET) ₁₈]	crystal structure	co-reduction, antialgalic exchange	48,76,92,135,136
72	Au _{25-x} Cu _x	phenylethanethiol	[Au _{25-x} Cu _x (PET) ₁₈]	mass spectrometry	co-reduction, antialgalic exchange	77,92,136
73	Ag _{55-x} Au _x	2,4-dichlorobenzenethiol/2,4-dimethylbenzenethiol	(PPh ₄) ₂ [Ag _{55-x} Au _x (SR) ₁₈]	crystal structure, mass spectrometry	co-reduction, galvanic exchange, intercluster reaction	60,137,138
74	Ag ₇ Au ₆	mercaptoposuccinic acid	Ag ₇ Au ₆ (H ₂ MSA)	mass spectrometry	galvanic exchange	37
75	Au _x Ag _{50-x}	<i>tert</i> -butyl benzylmercaptan 1,1-bis(diphenylphosphino)methane	Au _x Ag _{50-x} (DPPM) ₆ (SR) ₃₀ (R = TBBM)	crystal structure	galvanic exchange	139

Table 1. continued

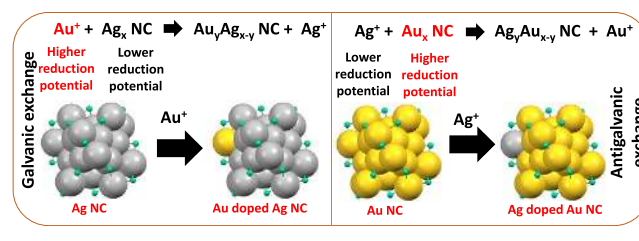
no	core	ligand	alloy cluster	focus	method of synthesis	reference
76	AuAg ₂₄	6-mercaptopentanoic acid	AuAg ₂₄ (MHA) ₁₈	mass spectrometry	galvanic exchange	140
77	Ag ₂₆ Au/Ag ₂₄ Au	2-ethylbenzenethiol	[Ag ₂₆ Au(2-EBT) ₁₈ (PPh ₃) ₆] ⁺ /[Ag ₂₄ Au(2-EBT) ₁₈] ⁻	crystal structure	galvanic exchange	141
78	Pt ₁ Ag ₁₂ Cu ₁₂ Au ₄	adamentanethiol	Pt ₁ Ag ₁₂ Cu ₁₂ Au ₄ (S-Adm) ₁₈ (PPh ₃) ₄	mass spectrometry	galvanic reduction	34
79	Au ₂₂ Ir ₃	phenylethylthiol	Au ₂₂ Ir ₃ (PET) ₁₈	mass spectrometry	intercluster reaction	142
80	Au ₁₂ Ag ₁₇	1,3-benzenedithiol, triphenylphosphine	Au ₁₂ Ag ₁₇ (BDT) ₁₂ (PPh ₃) ₄	mass spectrometry	intercluster reaction	89
81	MAu _x Ag _{38-x} (M = Ni/Pd)	1,3-benzenedithiol, triphenylphosphine	MAu _x Ag _{38-x} (BDT) ₁₂ (PPh ₃) ₄ (M = Ni/Pd/Pt)	mass spectrometry	intercluster reaction	89
82	Au ₂₀ Ag ₅	captropil	Au ₂₀ Ag ₅ (Capt) ₁₈	mass spectrometry	intercluster reaction	143
83	Ag _{51-x} Au _x	1,3-benzenedithiol	Ag _{51-x} Au _x (BDT) ₁₉ (PPh ₃) ₃	mass spectrometry	intercluster reaction	144
84	Ag ₁₃ Au ₁₂	triphenylphosphine, phenylethylthiol	[Ag ₁₃ Au ₁₂ (PPh ₃) ₁₀ (SR) ₅ Cl ₂] ²⁺	crystal structure	ligand exchange	54
85	PtAg ₂₈	1,3-benzenedithiol, triphenylphosphine	PtAg ₂₈ (BDT) ₁₂ (PPh ₃) ₄	crystal structure	ligand exchange	145,146
86	PdAg ₂₈	1,3-benzenedithiol, triphenylphosphine	PdAg ₂₈ (BDT) ₁₂ (PPh ₃) ₄	mass spectrometry	ligand exchange	89
87	NiAg ₂₈	1,3-benzenedithiol, triphenylphosphine	NiAg ₂₈ (BDT) ₁₂ (PPh ₃) ₄	mass spectrometry	ligand exchange	89
88	Au ₁₆ Ag	adamentanethiol	[Au ₁₆ Ag(S-Adm) ₁₃]	crystal structure	ligand exchange	95
89	PtAg ₁₂	1,1-bis(diphenylphosphino)methane, 2,4-dimethylbenzenethiol	PtAg ₁₂ (dppm) ₅ (SPHMe ₂) ₂	mass spectrometry	ligand exchange	147
90	Au ₄ Cu ₅	cyclohexanethiol, 1,1-bis(diphenylphosphino)methane	[Au ₄ Cu ₅ (C ₆ H ₁₁ S) ₆ (Dppm) ₂](BPh ₄)	crystal structure	ligand exchange	113
91	Au ₈ Ag ₅₅	1,3-bis(diphenylphosphino)propane, cyclohexanethiol, tetraphenylborate	[Au ₈ Ag ₅₅ (Dppp) ₄ (C ₆ H ₁₁ S) _{3,4}](BPh ₄) ₂	crystal structure	ligand exchange	114
92	PtAg ₈	adamentanethiol, triphenylphosphine	PtAg ₈ (S-Adm) ₁₈ (PPh ₃) ₄	crystal structure	ligand exchange	148
93	Au ₁ Ag ₂₂	adamentanethiol	[Au ₁ Ag ₂₂ (S-Adm) ₁₂] ³⁺	crystal structure	ligand exchange	149
94	Au _{24-x} Ag _x	<i>tert</i> -butyl benzylmercaptant	Au _{24-x} Ag _x (TBBM) ₂₀	crystal structure	ligand exchange	150
95	PtAg ₂₈	hexanethiol	PtAg ₂₈ (HT) ₁₈ (PPh ₃) ₄	crystal structure	ligand exchange	151
96	Ag ₂ Au ₂₅	phenylethylthiol	Ag ₂ Au ₂₅ (PET) ₁₈	mass spectrometry	metal deposition	152
97	MAu ₂₄ (M = Ag/Cu)	phenylethylthiol, triphenylphosphine	[MAu ₂₄ (PPh ₃) ₁₀ (PET) ₅ Cl ₁] ²⁺ (M = Ag/Cu)	crystal structure	metal deposition	153

procedure, a large number of bimetallic NCs and a few trimetallic NCs have been prepared. In 1984, the first phosphine-protected biicosahedral Au and Ag alloy NC was synthesized following co-reduction method by Teo and Keating. The obtained alloy NC contained 25 metal atoms with the molecular composition of $[(\text{PPh}_3)_{12}\text{Au}_{13}\text{Ag}_{12}\text{Cl}_6]^{m+}$.⁷¹ This work was followed by the synthesis of $[(\text{Ph}_3\text{P})_{10}\text{Au}_{13}\text{Ag}_{12}\text{Br}_8] \cdot (\text{PF}_6)$.⁷² Then, the same group found new triicosahedral and tetraicosahedral alloy NCs, $[(p\text{-Tol}_3\text{P})_{12}\text{Au}_{18}\text{Ag}_{20}\text{Cl}_{14}]$ and $[(\text{Ph}_3\text{P})_{12}\text{Au}_{22}\text{Ag}_{24}\text{Cl}_{10}]$, respectively.^{73,74} In 1994, Brust *et al.* reported the synthesis of thiolate-protected Au NCs, which showed more stability than their phosphine-protected analogs.⁷⁵ Among thiolate-protected NCs, $\text{Au}_{25}(\text{SR})_{18}$ is one of the most studied NCs due to its higher stability. In 2009, Murray *et al.* synthesized $\text{PdAu}_{24}(\text{PET})_{18}$, which was found to have different electrochemical properties than its monometallic analog.⁵⁷ Ag, Cu, and Pt atoms were incorporated into $\text{Au}_{25}(\text{PET})_{18}$ to make $\text{Au}_{25-x}\text{Ag}_x(\text{PET})_{18}$,⁷⁶ $\text{Au}_{25-x}\text{Cu}_x(\text{PET})_{18}$,⁷⁷ and $\text{PtAu}_{24}(\text{PET})_{18}$ ⁵⁵ *via* this method. Later, $\text{PdAu}_{24}(\text{DDT})_{18}$ (DDT = dodecanethiol) was purified by Negishi *et al.* using HPLC and the cluster was more stable than monometallic $\text{Au}_{25}(\text{DDT})_{18}$.⁷⁸ $\text{Au}_{25-r}\text{Ag}_r(\text{DDT})_{18}$ was also prepared and the number of doped Ag atoms was dependent on the molar ratio of the precursor salts.⁷⁹ Ni-doped bi- and trimetallic clusters such as Ag_4Ni and $\text{Ag}_{12}\text{Au}_{12}\text{Ni}$ were achieved by this method, which can exhibit interesting magnetic properties.^{18,80} Various other alloys with interesting properties can be synthesized easily. Such an example is the chiral alloy NC, $\text{Au}_{13}\text{Cu}_2((2r,4r)/(2s,4s)\text{-BDPP})_3(\text{SPy})_6$, which was synthesized using chiral ligand 2,4-bis(diphenylphosphino)pentane (BDPP).⁸¹ In addition, alloys of larger-sized NCs were also obtained such as $(\text{Ag-Au})_{144}(\text{PET})_{60}$, $\text{Au}_{144-x}\text{Cu}_x(\text{SC}_6\text{H}_{13})_{60}$, $[\text{Au}_{80}\text{Ag}_{30}(\text{PhC}\equiv\text{C})_{42}\text{Cl}_9]\text{Cl}$, etc.⁸²⁻⁸⁴ A large number of Ag-rich alloy NCs were also synthesized such as $[\text{Ag}_{46}\text{Au}_{24}(\text{TBHP})_{32}]^{2+}$, $(\text{TOA})_3\text{AuAg}_{16}(\text{TBTT})_{12}$, $\text{Au}_{12}\text{Ag}_{32}(\text{FTP})_{30}$, $\text{Ag}_{28}\text{Cu}_{12}(2,4\text{-DCBT})_{24}$, etc.^{31,85-87} Among various Ag NCs, $\text{Ag}_{25}(\text{DMBT})_{18}$ is one of the most studied Ag NCs due to its exceptional stability than other Ag NCs and it is structurally similar to $\text{Au}_{25}(\text{PET})_{18}$. Different groups have synthesized its Pt-, Pd-, and Au-doped alloys such as $\text{PtAg}_{24}(2,4\text{-DMBT})_{18}$, $\text{PdAg}_{24}(2,4\text{-DMBT})_{18}$, and $\text{Ag}_x\text{Au}_{25-x}(\text{PET})_{18}$.^{60,88} Our group has reported Ni-doped Ag_{25} , $\text{NiAg}_{24}(2,4\text{-DMBT})_{18}$.⁸⁹ Synthesis of alloy NCs using metal precursors having large differences in their redox potentials is difficult. Hence, the incorporation of Fe and Cd by co-reduction method is not possible. NaBH_4 is the most used reducing agent during the synthesis of bi- and trimetallic NCs. However, other reducing agents were used such as H_2 , which was used to prepare $[\text{Pt}(\text{H})(\text{PPh}_3)(\text{AuPPh}_3)_7]^{2+}$.⁹⁰ A list of NCs prepared so far (until September 2020) is given in Table 1, which includes co-reduction method.

3. GALVANIC REDUCTION METHOD

The post-synthetic metal exchange reaction of a NC with a suitable metal precursor is one of the important methods for the preparation of alloy NCs. Among different metal exchange reactions, galvanic reduction reaction has become a very effective approach for making multimetallic alloy NCs as well as various anisotropic alloy nanoparticles. According to the classic galvanic theory, a metal ion of higher reduction potential in solution gets reduced and replaces a metal atom present in a material and the latter subsequently enters the solution after being oxidized. The process is explained in detail in Scheme 2. The metal activity sequence is $\text{Fe} (-0.77 \text{ V}) > \text{Cd} (-0.40 \text{ V}) >$

Scheme 2. Schematic Representation of Galvanic and Antigalvanic Exchange Reaction Processes Using Au and Ag as Examples

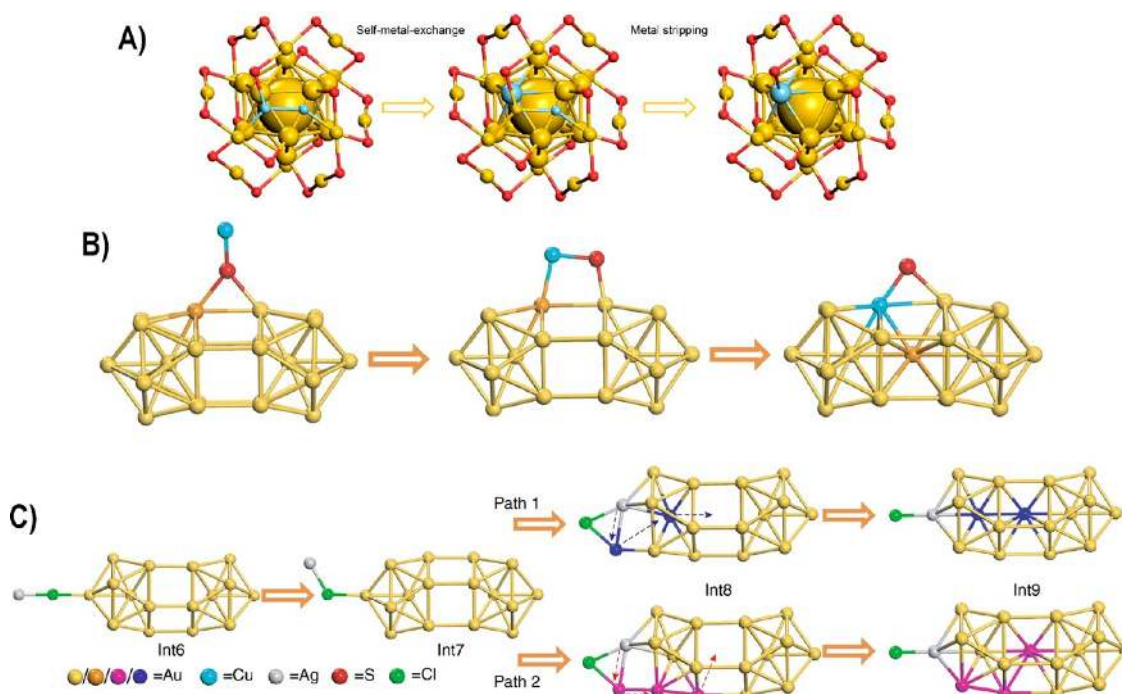


$\text{Co} (-0.28 \text{ V}) > \text{Ni} (-0.25 \text{ V}) > \text{Cu} (+0.34 \text{ V}) > \text{Hg} (+0.79 \text{ V}) > \text{Ag} (+0.80 \text{ V}) > \text{Pd} (+0.95 \text{ V}) > \text{Pt} (+1.2 \text{ V}) > \text{Au} (+1.50 \text{ V})$. Various metal atoms have been incorporated in the Ag NCs using galvanic replacement procedure to make silver-rich multimetallic alloy NCs. Such an example is the atomically precise doping of Au atom in $\text{Ag}_{25}(\text{DMBT})_{18}$ to make $\text{Ag}_{24}\text{Au}(\text{DMBT})_{18}$ (reduction potentials of Ag^+/Ag and Au^+/Au are 0.80 and 1.69 V, respectively).¹³⁷ It was found that co-reduction led to the synthesis of $\text{Ag}_{25-x}\text{Au}_x(\text{DMBT})_{18}$ (where $x = 1-8$) and, therefore, it is difficult to make single crystals. The availability of single crystal will help in understanding the position of the dopant and, hence, synthesis of a single product is important, which can be achieved by this method. $\text{Ag}_{24}\text{Au}(\text{DMBT})_{18}$ exhibits higher stability and enhanced photoluminescence than monometallic $\text{Ag}_{25}(\text{DMBT})_{18}$. For the synthesis of $\text{Ag}_{24}\text{Au}(\text{DMBT})_{18}$, an already synthesized $\text{Ag}_{25}(\text{DMBT})_{18}$ was treated with AuClIPPh_3 , which changed the color of the solution from brown to green. The product was characterized using ESI MS and SCXRD. The structure of bimetallic $\text{Ag}_{24}\text{Au}(\text{DMBT})_{18}$ is similar to the monometallic one. During galvanic exchange reaction, the structure of monometallic NC remains unaltered in their multimetallic analogue; however, Kang *et al.* reported shape-altered synthesis of alloy NCs using this method.⁴⁰ The incorporation of Au atoms in $\text{PtAg}_{24}(\text{DMBT})_{18}$ resulted in the formation of shape-unaltered trimetallic $\text{PtAu}_x\text{Ag}_{24-x}(\text{DMBT})_{18}$ when Au-DMBT was used as the precursor, while the use of AuBrPPh_3 led to the formation of shape-altered trimetallic $\text{Pt}_2\text{Au}_{10}\text{Ag}_{13}(\text{PPh}_3)_{10}\text{Br}_7$. In this case, Br^- peeled away the PtAg_{12} core from the staple motifs and transformed it into a biicosahedron, which was stabilized by PPh_3 ligand instead of DMBT. Trimetallic $\text{PtCu}_x\text{Ag}_{28-x}(\text{BDT})_{12}(\text{PPh}_3)_4$ and tetrametallic $\text{Pt}_1\text{Ag}_{12}\text{Cu}_{12}\text{Au}_4(\text{S-Adm})_{18}(\text{PPh}_3)_4$ (S-Adm = adamantaneethiol) NCs were synthesized by galvanic replacement procedure. Several bimetallic NCs have been prepared *via* this method, which are listed in Table 1.

4. ANTIGALVANIC EXCHANGE REACTION

Alloying or doping in $\text{Au}_{25}(\text{SR})_{18}$ was performed largely with different metals such as Ag, Cu, Pd, Pt, Ni, Cd, Hg, and Ir. According to the classic galvanic reduction method, Au NCs are unable to react with the less noble metal atoms such as Ag, Cu, Cd, etc. (reduction potentials of Au^+/Au , Ag^+/Ag , Cu^{2+}/Cu , and Cd^{2+}/Cd are +1.50, +0.80, +0.34, and -0.40 V , respectively). However, Murray *et al.* showed the reduction of Ag ions by Au NCs, which was followed by the replacement of Au atoms with Ag, leading to the formation of $\text{Ag}_x\text{Au}_{25-x}(\text{SR})_{18}$ alloy NCs.¹³⁵ This reaction was named as antigalvanic reduction, which is a unique property of Au and Ag NCs and nanoparticles of core size below 3 nm.¹³⁶ In 2012, Wu performed the reaction between $\text{Au}_{25}(\text{PET})_{18}$ and Ag ions and the formed bimetallic

Scheme 3. Mechanistic pathway of the conversion of $\text{Ag}_2\text{Au}_{25}(\text{SR})_{18}$ to $\text{AgAu}_{25}(\text{SR})_{18}$ and Proposed Mechanisms of Cu and Ag Atom Deposition in $[\text{Au}_{24}(\text{PPh}_3)_{10}(\text{PET})_5\text{Cl}_2]^+$.^a



Adapted from refs 152 and 153. Copyright 2018 Nanomaterials and 2017 Nature^a (A) Mechanistic pathway of the conversion of $\text{Ag}_2\text{Au}_{25}(\text{SR})_{18}$ to $\text{AgAu}_{25}(\text{SR})_{18}$. Color codes: red, yellow, and cyan colors denote S, Au, and Ag atoms, respectively. (B, C) Proposed mechanisms of Cu and Ag atom deposition in $[\text{Au}_{24}(\text{PPh}_3)_{10}(\text{PET})_5\text{Cl}_2]^+$, which resulted in the synthesis of $[\text{MAu}_{24}(\text{PPh}_3)_{10}(\text{PET})_5\text{Cl}_2]^{2+}$ ($M = \text{Cu}/\text{Ag}$). Color codes: yellow, orange, pink, and navy blue colors denote Au atoms, while cyan, gray, red, and green colors denote Cu, Ag, S, and Cl, respectively.

products were characterized using laser desorption ionization (LDI) MS. To prove that antialgal exchange reaction is not a unique property of $\text{Au}_{25}(\text{PET})_{18}$ NC, approximately 2–3 nm nanoparticles were treated with AgNO_3 solution. The incorporated Ag was detected by XPS and, after the reaction, the binding energy of Ag indicated the incorporation of neutral Ag, which confirmed the reduction of Ag ions by Au nanoparticles. A similar experiment was performed on 3 nm-sized Ag nanoparticles using Cu salt and incorporation of neutral Cu in Ag nanoparticles was observed using XPS. This proved that Cu ions can be reduced by more noble Ag atoms. Antialgal reduction reaction is feasible due to the enhanced reducing ability when the metal is in nanoscale form. One of the important driving factors for antialgal reduction is the protective ligands on the surface of nanoparticles or NCs. It was proposed that the partial negative charge present on the surface ligands plays a crucial role in the reduction of more reactive ions. This observation led Wu *et al.* to modify the sequence of metal activity as $\text{Fe} > \text{Ni} > \text{Pd} > \text{Au} (\sim 3 \text{ nm}) > \text{Cu} > \text{Ag}$.^{92,136} After that, Zhu *et al.* showed the incorporation of monovalent Cu/Ag and bivalent Cd/Hg in $\text{Au}_{25}(\text{SR})_{18}$ NCs.⁹¹ Cd and Hg atoms were getting doped at the center of the icosahedral core, while Cu and Ag atoms were incorporated on the surface of the icosahedron. Similar to galvanic exchange reaction, in the case of antialgal exchange, dopants are mostly getting incorporated in the parent NCs without changing their structures and compositions. However, in some NC systems, the replacement with a foreign metal atom can lead to structural transformations. For example, the doping of Ag and Cu atoms in $\text{Au}_{25}(\text{SR})_{18}$, $\text{Au}_{38}(\text{PET})_{24}$, $\text{Au}_{36}(\text{SR})_{24}$, $\text{Au}_{144}(\text{PET})_{60}$, etc., and doping of Cd and Hg in $\text{Au}_{25}(\text{SR})_{18}$ resulted in the formation of alloy NCs

with preserved composition and structure.^{82,91,97,132} On the other hand, doping of Ag atoms in $\text{Au}_{23}(\text{CHT})_{16}$ (CHT = cyclohexylthiol) NCs first led to the formation of $\text{Au}_{23-x}\text{Ag}_x(\text{CHT})_{16}$, which then got converted to $\text{Au}_{25-x}\text{Ag}_x(\text{CHT})_{18}$.^{38,154} The Au-rich trimetallic and tetrametallic NCs $\text{M}_1\text{Ag}_x\text{Au}_{24-x}(\text{SR})_{18}$ ($M = \text{Cd}/\text{Hg}$)⁴¹ have also been synthesized by this effective method. A list of multicomponent NCs made *via* antialgal reduction is presented in Table 1.

5. METAL DEPOSITION METHOD

The metal deposition or intramolecular metal exchange is one of the emerging alloying methods. Li *et al.* reported the synthesis of $\text{Ag}_2\text{Au}_{25}(\text{SR})_{18}$ *via* reaction of $\text{Au}_{25}(\text{SR})_{18}$ with AgNO_3 ¹⁵² where Ag atoms occupied the outer staple. But, after treatment with excess ligand, Ag atoms diffused within the icosahedral core, which led to the formation of $\text{AgAu}_{24}(\text{SR})_{18}$. The reaction occurred in two steps as shown in Scheme 3A. The first step is the self-metal exchange, which is the intramolecular metal exchange. During the first step, one of the Ag atoms, which were in the outer staple (denoted in blue color in Scheme 3A), got exchanged with one of the icosahedral Au atoms. Thus, after exchange, one Ag atom was on the inner icosahedral surface and another one in the outer staple. This was followed by the second step where the surface Au and Ag atoms were detached from the surface of the cluster and resulted in the synthesis of $\text{AgAu}_{24}(\text{SR})_{18}$. This process was called the metal stripping process. The same process was observed by Zheng *et al.* in $\text{AuAg}_{24}(\text{MHA})_{18}$ NCs.¹⁴⁰

Using high-resolution ESI MS, they monitored real-time diffusion of Au atoms from the staple motif to the icosahedral surface and then to the center of the icosahedron to attain

thermodynamic stability. The metal deposition method can be extrapolated into a hollowing and refilling process where foreign metal atoms are incorporated to make alloy NCs. Single Cu and Ag atoms were added successfully by Wang *et al.* in $[\text{Au}_{24}(\text{PPh}_3)_{10}(\text{PET})_5\text{Cl}_2]^+$, which led to the synthesis of $[\text{MAu}_{24}(\text{PPh}_3)_{10}(\text{PET})_5\text{Cl}_2]^{2+}$ ($M = \text{Ag}/\text{Cu}$).¹⁵³ In this case, the $-\text{SR}$ group and Cl atom played important roles. At first, a foreign atom got attached to the S/Cl atom present in the waist/apex positions, respectively. Due to this interaction, the Au–S/Au–Cl bond collapsed and the Au atom migrated to the central position, which reduced the energy of the system as shown in Scheme 3B,C. Mainly, the Ag atom was doped at the apex site, while Cu occupied both apex and waist positions as the Ag–Cl bond is stronger than Ag–SR, unlike that of Cu–Cl that has the same binding energy as of Cu–SR.

6. LIGAND EXCHANGE METHOD

Ligand exchange is an efficient method for the synthesis of atomically precise NCs in which one NC is converted to another, with the same or different nuclearity in the presence of foreign ligands.⁶⁸ The ligand exchange process where the structure of the starting NC undergoes structural transformation is named as ligand exchange-induced structural transformation (LEIST) by Jin's group.¹⁵⁵ This is a fast-evolving method in NC chemistry, which enhances the range of applications of NCs by introducing different functional ligands. LEIST method has been widely used for making a large number of monometallic NCs; however, it is now also being used for the preparation of multimetallic NCs. Biicosahedral $\text{Pt}_2\text{Ag}_{23}(\text{PPh}_3)_{10}\text{Cl}_7$ was converted to monoicosahedral $\text{PtAg}_{24}(\text{DMBT})_{18}$ and $\text{PtAg}_{28}(\text{BDT})_{12}(\text{PPh}_3)_4$ on addition of DMBT and BDT ligands, respectively.^{145,147} $\text{PtAg}_{28}(\text{S-Adm})_{18}(\text{PPh}_3)_4$ was synthesized by the conversion of $\text{PtAg}_{24}(\text{DMBT})_{18}$ after addition of Adm-SH and PPh_3 .¹⁴⁸ Similarly, $\text{MAG}_{28}(\text{BDT})_{12}(\text{PPh}_3)_4$ ($M = \text{Ni}/\text{Pd}/\text{Pt}$) was synthesized *via* the LEIST method starting from $\text{MAG}_{24}(\text{DMBT})_{18}$ ($M = \text{Ni}/\text{Pd}/\text{Pt}$) (see Figure 1).⁸⁹ Ligand exchange method also helped make the *n*-hexanethiol (HT)-protected NC, $\text{PtAg}_{28}(\text{HT})_{18}(\text{PPh}_3)_4$ from $\text{PtAg}_{28}(\text{S-Adm})_{18}(\text{PPh}_3)_4$, keeping the structure unaltered.¹⁵¹ Moreover, Zhu *et al.* showed the synthesis of highly luminescent $\text{Pt}_1\text{Ag}_{12}(\text{dppm})_5(\text{DMBT})_2$ from feebly luminescent $\text{Pt}_2\text{Ag}_{23}(\text{PPh}_3)_{10}\text{Cl}_7$ by introducing dppm along with DMBT.¹⁴⁷ Further, Kang *et al.* reported a new alloy NC, $\text{AgAu}_{16}(\text{S-Adm})_{13}$ starting from $\text{AgAu}_{17}(\text{CHT})_{14}$ by this methodology.⁹⁵ Also, $\text{Ag}_x\text{Au}_{24-x}(\text{TBBT})_{16}$ was synthesized from $\text{Ag}_x\text{Ag}_{23-x}(\text{HT})_{16}$ upon treatment with TBBT. It has been proposed that the drastic change in the nuclearity of the NC is due to the change in the electron-withdrawing and electron-donating effect of ligands, which depends on the position of the functional groups. The noncovalent interactions and steric hindrance are also crucial factors for this transformation. However, the effect of ligand on the nuclearity and structure of the NC is unclear.

7. INTERCLUSTER REACTION METHOD

Besides various synthetic methods, the reaction between two NCs has become an emerging method to obtain multimetallic alloy NCs. We are discussing this method more elaborately than others as it has not been reviewed previously, in the context of alloy clusters. Krishnadas *et al.* found the chemical reaction between two atomically precise NCs, which resembles the reaction between two organic molecules. They first reported the

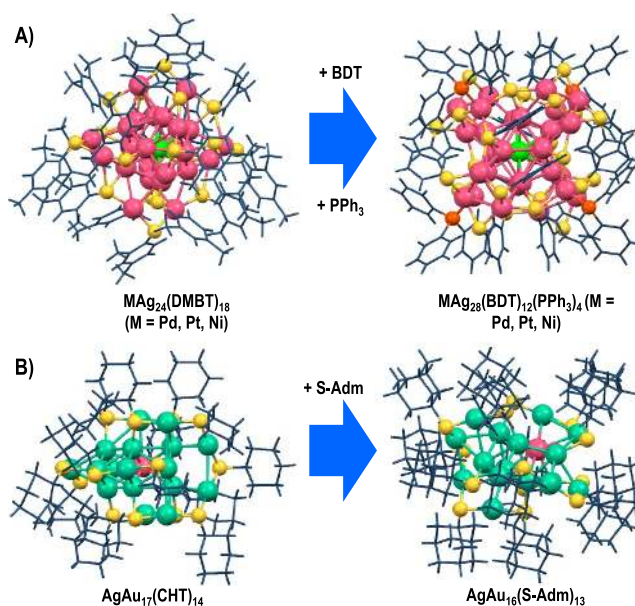


Figure 1. (A) Formation of $\text{MAG}_{28}(\text{BDT})_{12}(\text{PPh}_3)_4$ from $\text{MAG}_{24}(\text{DMBT})_{18}$ ($M = \text{Pd}, \text{Pt}, \text{Ni}$) NCs. Green, pink, yellow, and orange denote M (Pd, Pt, Ni), Ag, S, and P atoms, respectively. Blue color denotes C and H atoms of thiol ligands. (B) Conversion of $\text{AgAu}_{17}(\text{CHT})_{14}$ to $\text{AgAu}_{16}(\text{S-Adm})_{13}$. The colors pink, green, and yellow denote Ag, Au, and S atoms, respectively. Blue color denotes C and H atoms of thiol ligands.

reaction between pure Ag and Au NCs, $\text{Ag}_{44}(\text{FTP})_{30}$ and $\text{Au}_{25}(\text{FTP})_{18}$, respectively, which led to the formation of Au-doped $\text{Ag}_{44}(\text{FTP})_{30}$ and Ag-doped $\text{Au}_{25}(\text{FTP})_{18}$ bimetallic NCs.¹³⁸ These intercluster reactions are controlled by both kinetics and thermodynamics. The extent of reaction and its mechanism were studied in detail using MS. Negative-mode MALDI MS at two different reaction times at the $\text{Au}_{25}(\text{FTP})_{18}$ side is shown in Figure 2. The blue spectrum corresponding to MALDI MS after 1 h of reaction showed the incorporation of up to 5 Ag atoms, which resulted in the formation of $\text{Au}_{25-x}\text{Ag}_x(\text{FTP})_{18}$, while the insertion of up to 13 Ag atoms was observed after 3 h of reaction (red spectrum). As both reacting NCs were protected by the same protecting ligand, no

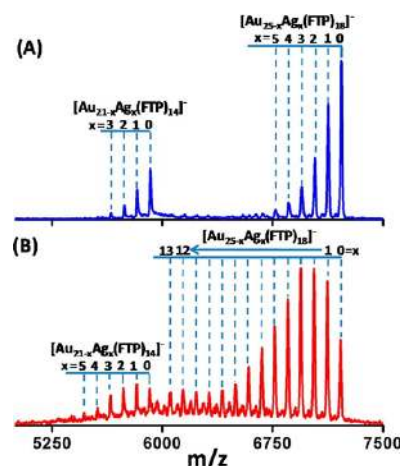


Figure 2. MALDI MS of reaction between $\text{Au}_{25}(\text{FTP})_{18}$ and $\text{Ag}_{44}(\text{FTP})_{30}$ in negative ion mode after (A) 1 h and (B) 3 h of the reaction at the Au_{25} region. Reprinted from ref 138. Copyright 2016 American Chemical Society.

ligand exchange was observed in the MS. The doping of Ag atoms into $\text{Au}_{25}(\text{SR})_{18}$ was found to be more facile *via* this protocol where up to 20 Ag atoms can be incorporated. The total number of atoms and the overall charge state remain preserved in the formed alloy NCs during this kind of substitution reaction. Similar to the Au_{25} region, the reaction also occurred in the Ag_{44} region as shown in Figure 3.¹³³ At first, a mixture of bimetallic

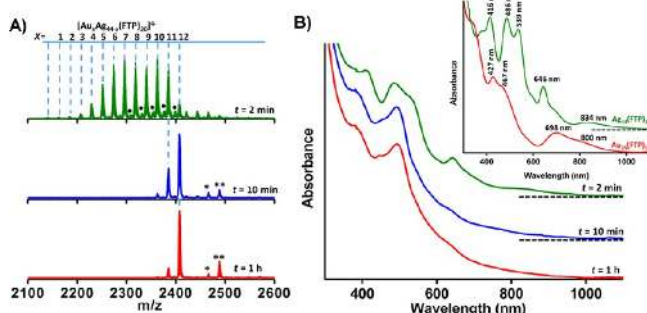


Figure 3. (A) Time-dependent ESI MS and (B) time-dependent UV–vis absorption spectra of the reaction between $\text{Ag}_{44}(\text{FTP})_{30}$ and $\text{Au}_{25}(\text{FTP})_{18}$ at the Ag_{44} region. Adapted from ref 133. Copyright 2017 American Chemical Society.

NCs was formed having the composition, $\text{Au}_x\text{Ag}_{44-x}(\text{FTP})_{30}$ where $x = 1-12$. After 1 h, this mixture resulted in the formation of $\text{Au}_{12}\text{Ag}_{32}(\text{FTP})_{30}$ exclusively (Figure 3A). The reaction was monitored by time-dependent UV–vis spectroscopy as shown in Figure 3B. It showed a significant spectral change with time and the final spectrum was completely different than that of $\text{Ag}_{44}(\text{FTP})_{30}$ as well as $\text{Au}_{25}(\text{FTP})_{18}$, confirming the formation of the bimetallic NC $\text{Au}_{12}\text{Ag}_{32}(\text{FTP})_{30}$. Although tools like MS, UV–vis absorption spectroscopy, NMR, etc., help in understanding the extent of doping, the precise structural insight can be obtained only from X-ray crystallography. In the absence of a single crystal, one can understand the doping position by computations as the structures of the monometallic NCs remain preserved to a large extent in the multimetallic NCs during such reactions. The single-crystal X-ray structure of $\text{Ag}_{44}(\text{FTP})_{30}$ consists of a Ag_{12} hollow icosahedron inside a Ag_{20} dodecahedron, which is covered by a $\text{Ag}_{12}(\text{FTP})_{30}$ outer shell. On the other hand, $\text{Au}_{25}(\text{FTP})_{18}$ is made up of a Ag_{13} central icosahedron protected by a $\text{Ag}_{12}(\text{FTP})_{18}$ surface motif. In the case of the reaction involving $\text{Ag}_{44}(\text{FTP})_{30}$ and $\text{Au}_{25}(\text{FTP})_{18}$, the total energy of the substituted product was found to be the most negative when Au and Ag atoms occupied the icosahedral surface of $\text{Ag}_{44}(\text{FTP})_{30}$ and $\text{Au}_{25}(\text{FTP})_{18}$, respectively. Hence, it was concluded that the substitution of metal atoms during the intercluster reaction was an energy-driven process. It was proposed that the intercluster reaction proceeds through bond breaking due to metallophilic and noncovalent interactions between ligands or redox reactions. The fragments generated after bond breaking behaved as nucleophiles, which led to the incorporation of another metal atom similar to that of the metal exchange reactions. The formation of an adduct of two NCs (due to noncovalent interactions between ligands and metallophilic interactions) was observed in ESI MS during the reaction between two structurally similar Au and Ag NCs, $\text{Au}_{25}(\text{PET})_{18}$ and $\text{Ag}_{25}(\text{DMBT})_{18}$, as shown in Figure 4.¹⁵⁶ The adduct vanished within 5 min of mixing and a series of peaks were observed due to the formation of $\text{Au}_x\text{Ag}_y(\text{SR})_{18}$. This adduct formation suggested that the intercluster reaction is

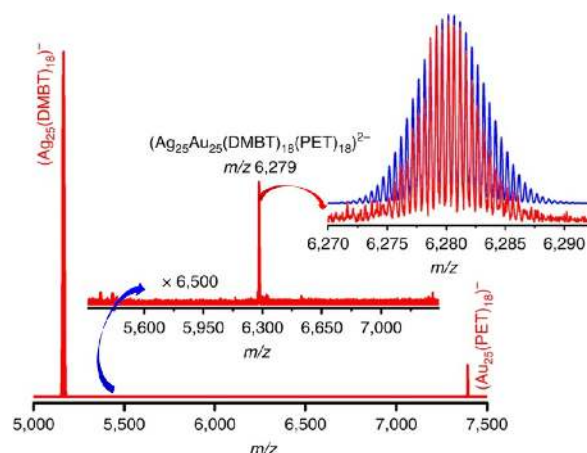


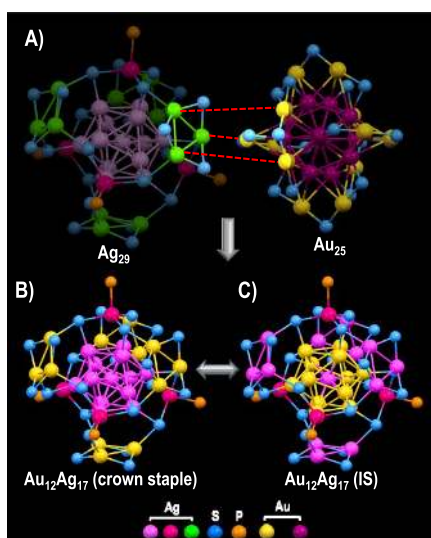
Figure 4. ESI MS of the mixture of $[\text{Ag}_{25}(\text{DMBT})_{18}]^-$ and $[\text{Au}_{25}(\text{PET})_{18}]^-$, resulting in the formation of the intermediate adduct $[\text{Ag}_{25}\text{Au}_{25}(\text{DMBT})_{18}(\text{PET})_{18}]^{2-}$ whose theoretical and experimental isotopic distributions match with each other. Reprinted from ref 156. Copyright 2016 Nature.

bimolecular. The structure of this adduct was calculated using DFT, which manifested that bond lengths of both NCs were longer than that of individual NCs. Also, the bond angles of staples of both NCs changed significantly in the adduct. Further chemical and structural transformation might occur during the reaction after adduct formation. In the alloy NCs $\text{Au}_x\text{Ag}_y(\text{SR})_{18}$, the number of doped Ag and Au atoms can be varied from 1 to 24 by varying the molar ratio of reactant NCs. Therefore, the desired number of dopants can be inserted using intercluster reaction. Similar to the previous reaction, in this case, the total number of metal and ligand in alloy NCs is identical with that of the unreacted NCs. Regarding the dopant position, the computational study revealed that the total energy of the reaction will be the most favorable when a Au atom occupies the central position of the icosahedron in $\text{Ag}_{25}(\text{DMBT})_{18}$, while a Ag atom occupies the icosahedral surface of $\text{Au}_{25}(\text{PET})_{18}$. Not only Ag but also Ir metal incorporation in $\text{Au}_{25}(\text{SR})_{18}$ was obtained *via* intercluster reaction, which otherwise is difficult to achieve by other methods. Bhat *et al.* discussed the intercluster reaction between an Ir NC, $\text{Ir}_9(\text{PET})_6$, and a Au NC, $\text{Au}_{25}(\text{PET})_{18}$, which led to the formation of $\text{Ir}_3\text{Au}_{22}(\text{PET})_{18}$.¹⁴² In this reaction, only one single product got formed, which was then separated from the unreacted NCs by thin-layer chromatography (TLC), and the purity was checked with ESI MS. The DFT study revealed that the Ir atoms occupy the center and surface of the icosahedral core.

In these reactions, the use of two monothiol-protected NCs also led to ligand exchange; although, the total number of thiol ligands remains the same. As DMBT and PET are of the same mass, no ligand exchange could be observed in ESI MS data but ligand exchange between FTP and PET was observed. Due to high mobility, ligands undergo spontaneous exchange. The mobility of ligands can be decreased by using bidentate ligands such as dithiols. Ghosh *et al.* showed the reactions of bidentate thiol-protected NCs, $\text{Ag}_{51}(\text{BDT})_{19}(\text{PPh}_3)_3$ and $\text{Ag}_{29}(\text{BDT})_{12}(\text{PPh}_3)_4$, with $\text{Au}_{25}(\text{PET})_{18}$ and noticed the exchange between Ag and Au atoms and no exchange occurred between the ligands.¹⁴⁴ The reaction rate was observed to be slow, which may be due to the presence of a rigid bidentate ligand that rigidifies the surface of the NC. They found the incorporation of three Au atoms in $\text{Ag}_{51}(\text{BDT})_{19}(\text{PPh}_3)_3$ and

$\text{Ag}_{29}(\text{BDT})_{12}(\text{PPh}_3)_4$. Later on, the reaction between $\text{Ag}_{29}(\text{BDT})_{12}(\text{PPh}_3)_4$ and $\text{Au}_{25}(\text{PET})_{18}$ was studied in detail, which showed the incorporation of a maximum of 12 Au atoms in $\text{Ag}_{29}(\text{BDT})_{12}(\text{PPh}_3)_4$, while only up to 7 Ag atoms were getting doped in $\text{Au}_{25}(\text{PET})_{18}$, unlike the previously mentioned intercluster reactions.⁸⁹ This was due to the use of a very high concentration of $\text{Au}_{25}(\text{PET})_{18}$ (five times higher) in comparison to $\text{Ag}_{29}(\text{BDT})_{12}(\text{PPh}_3)_4$ to increase the reaction rate, which was otherwise very slow due to the rigid surface. This proved that the rate of reactions strongly depends on the metal–ligand interface. The oligomeric M_xL_y surface staples were well defined in these NCs, and in some of these clusters, the oligomeric staple motifs formed interlocked rings as in $\text{Ag}_{25}(\text{SR})_{18}$ and $\text{Au}_{25}(\text{SR})_{18}$. The structure of these kinds of NCs had been compared to the Borromean rings, as proposed by Natarajan *et al.*, and NCs were referred to as aspicules (meaning shielded molecules).¹⁵⁷ According to this structural alignment, breaking of one ring led to the destruction of the entire structure of these NCs, which resulted in the generation of M_xL_y fragments behaving as nucleophiles in the substitution reaction. This process led to the incorporation of 1–24 Ag and Au atoms in the respective NCs to make bimetallic ones. This was not the same in the case of dithiol-protected NCs such as in $\text{Ag}_{29}(\text{BDT})_{12}(\text{PPh}_3)_4$, which comprised two types of staples: Ag_3S_6 and Ag-P, unlike that of the Borromean ring structure. These staples were difficult to break as they were stabilized by dithiol, and hence, it was proposed that $\text{Au}_{25}(\text{SR})_{18}$ NCs were interacting with $\text{Ag}_{29}(\text{BDT})_{12}(\text{PPh}_3)_4$ *via* weak van der Waal interactions at the less congested Ag_3S_6 staples as shown in Scheme 4. This interaction assisted the metal exchange between two NCs at the outer staple, leading to the synthesis of bimetallic NCs. Then, the doped Ag and Au atoms underwent intramolecular galvanic

Scheme 4. Proposed Interactions between Ag and Au Atoms of $\text{Ag}_{29}(\text{BDT})_{12}(\text{PPh}_3)_4$ and $\text{Au}_{25}(\text{PET})_{18}$ (A), Which Led to the Formation of Kinetically Controlled $\text{Au}_{12}\text{Ag}_{17}(\text{BDT})_{12}(\text{PPh}_3)_4$ at the Outer Surface, Which Then Diffuses Inside the Icosahedron Core to Form a Thermodynamically Stable Structure.⁸⁹



Adapted with permission from ref 89. Copyright 2020 American Chemical Society “Color codes: Green and pink (both light and dark shades) denote Ag atoms, yellow and purple denote Au atoms, cyan denotes S atoms, and orange denotes P atoms.

and antialgal exchange to occupy the energetically most stable positions, which were the icosahedral surface positions.

Intercluster reaction was then expanded to make trimetallic NCs.⁸⁹ We showed the reaction of bimetallic $\text{MAg}_{28}(\text{BDT})_{12}(\text{PPh}_3)_4$ (where $\text{M} = \text{Ni}/\text{Pd}/\text{Pt}$) with monometallic $\text{Au}_{25}(\text{PET})_{18}$, which produced a mixture of trimetallic $\text{MAu}_x\text{Ag}_{28-x}(\text{BDT})_{12}(\text{PPh}_3)_4$ and bimetallic $\text{Ag}_x\text{Au}_{25-x}(\text{PET})_{18}$. Unlike $\text{Ag}_{29}(\text{BDT})_{12}(\text{PPh}_3)_4$, the use of doped $\text{Ag}_{29}(\text{BDT})_{12}(\text{PPh}_3)_4$ exhibited higher reactivity; however, it was slower as compared to the monothiol-protected ones. A time-dependent ESI MS of the reaction sequence between $\text{PdAg}_{28}(\text{BDT})_{12}(\text{PPh}_3)_4$ and $\text{Au}_{25}(\text{PET})_{18}$ (1:5 molar ratio) is shown in Figure 5, which manifests the extent of reaction with time. With increasing time, the number of doped Au atoms increased and it formed a stable single trimetallic NC $\text{PdAu}_{12}\text{Ag}_{16}(\text{BDT})_{12}(\text{PPh}_3)_4$, while doping up to 7 Ag atoms was seen in $\text{Au}_{25}(\text{PET})_{18}$ forming a mixture of bimetallic $\text{Ag}_x\text{Au}_{25-x}(\text{PET})_{18}$ (where $x = 1-7$) clusters. Similar to $\text{PdAu}_{12}\text{Ag}_{16}(\text{BDT})_{12}(\text{PPh}_3)_4$, trimetallic $\text{PtAu}_{12}\text{Ag}_{16}(\text{BDT})_{12}(\text{PPh}_3)_4$ NC too got formed by intercluster reaction between $\text{PtAg}_{28}(\text{BDT})_{12}(\text{PPh}_3)_4$ and $\text{Au}_{25}(\text{PET})_{18}$. Also, $\text{NiAu}_x\text{Ag}_{28-x}(\text{BDT})_{12}(\text{PPh}_3)_4$ was obtained by intercluster reaction between $\text{NiAg}_{28}(\text{BDT})_{12}(\text{PPh}_3)_4$ and $\text{Au}_{25}(\text{PET})_{18}$. One important aspect to notice here was that the centrally doped Ni, Pd, and Pt atoms in $\text{Ag}_{29}(\text{BDT})_{12}(\text{PPh}_3)_4$ did not get transferred to $\text{Au}_{25}(\text{PET})_{18}$ to make corresponding bi- or trimetallic NCs. This observation supported the above mechanism, which depicted the involvement of metal–ligand interface during the intercluster reaction and not the central atom. Hence, based on this, we calculated the structure of trimetallic $\text{MAu}_{12}\text{Ag}_{16}(\text{BDT})_{12}(\text{PPh}_3)_4$ ($\text{M} = \text{Ni}/\text{Pd}/\text{Pt}$), where M atom was at the center of the icosahedral core and 12 Au atoms occupied the icosahedral surface positions.

There have been other attempts of intercluster reactions by other groups such as Xia *et al.*, who reported the synthesis of $\text{Au}_{20}\text{Ag}_5(\text{Capt})_{18}$ by the reaction between $\text{Au}_{25}(\text{Capt})_{18}$ and $\text{Ag}_{30}(\text{Capt})_{18}$.¹⁴³ The product was purified using polyacrylamide gel electrophoresis (PAGE). While both the reactant NCs were non-emissive, the alloy cluster exhibited intense red emission. MALDI MS was used to determine the composition of as-synthesized alloy NCs.

The reaction of nanocluster has also been observed with nanoparticles by Xia *et al.*¹⁴³ They found the doping of Cu atoms by the reaction of $\text{Au}_{25}(\text{SR})_{18}$ with Cu nanoparticles of ~ 1.4 nm. This gave a new turn of the reaction involving nanoclusters. Similarly, Bose *et al.* have observed doping of Ag atoms in atomically precise $\text{Au}_{25}(\text{PET})_{18}$ nanoclusters using polydispersed Ag nanoparticles.¹⁵⁸

8. NANOCUSTER-BULK REACTIONS

To understand the mechanism of intercluster reactions and the role of metal–ligand interfaces in greater detail, Kazan *et al.* conducted a reaction of NCs with surfaces of bulk metals.¹⁵⁹ They used $\text{Au}_{25}(\text{PET})_{18}$ and $\text{Au}_{38}(\text{PET})_{24}$ NCs to react with Ag, Cu, and Cd foils before and after functionalization with thiols. The doping rate was observed to be different for the treated and untreated foils. Treated Ag foils exhibited a faster reaction rate, which decreased with time, while the untreated one showed a lower reaction rate at first and slowly increased after a certain time. This observation indicated that pre-functionalized thiols on the foils play a crucial role in the reaction, which indeed emphasized the importance of metal–ligand interfaces during the reaction between NCs (the mechanism is shown in Scheme

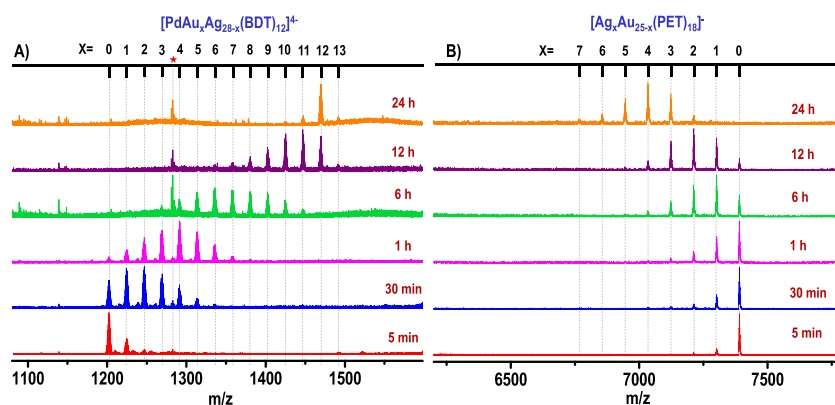
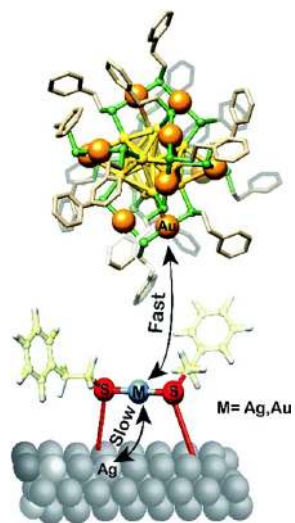


Figure 5. ESI MS of reaction between $\text{PdAg}_{28}(\text{BDT})_{12}(\text{PPh}_3)_4$ and $\text{Au}_{25}(\text{PET})_{18}$ (1:5 molar ratio) at different time intervals. (A) Reaction at the $\text{PdAg}_{28}(\text{BDT})_{12}(\text{PPh}_3)_4$ side and (B) the reaction at the $\text{Au}_{25}(\text{PET})_{18}$ side. The formed clusters are $[\text{PdAu}_x\text{Ag}_{28-x}(\text{BDT})_{12}]^{4-}$ and $[\text{Ag}_x\text{Au}_{25-x}(\text{PET})_{18}]^-$. The charged species are not mentioned in the text for simplicity. The red asterisk in (A) is due to thiolates produced during the reaction. Adapted with permission from ref 89. Copyright 2020 American Chemical Society.

5).¹⁶⁰ In the case of Cu and Cd foils, the reaction did not occur with the bare metal foils. Insertion of a few Cu and Cd atoms can

Scheme 5. Pictorial Illustration of the Reaction between $\text{Au}_{25}(\text{PET})_{18}$ with Ag Foil. Adapted with permission from ref 159. Copyright 2019 Royal Society of Chemistry



be seen during the reaction with the pre-treated foils. This new class of reactions of NCs with bulk metals opens up new opportunities for making different alloy NCs.

9. CONCLUSIONS AND FUTURE PERSPECTIVES

In the following, we list below several possibilities to expand this science.

Diversity: About 100 bimetallic alloy NCs are known till now; however, only about 10 alloy NCs with more than one heteroatom have been reported. To the best of our knowledge, only two tetrametallic NCs ($[\text{Pt}_1\text{Ag}_{12}\text{Cu}_{12}\text{Au}_4(\text{S-Adm})_{18}(\text{PPh}_3)_4]$ and $\text{Au}_{24-x-y}\text{Ag}_x\text{Cu}_y\text{Pd}(\text{SC}_{12}\text{H}_{25})_{18}$) have been reported. Hence, incorporation of more metals in a given cluster core, such as pentametallic and beyond, will be worth exploring. This may lead to high entropy alloy NCs, which might show improved properties, in areas such as catalysis. Finding some

methods to control the number of doped atoms in an alloy NC are also important.

The reaction of a NC with another NC of a different metal or even bulk metal is an efficient method for preparing bimetallic and trimetallic NCs. The reactions between a few NCs have been studied. There are more than 150 NCs whose structures have been solved and many more NCs are reported, whose structures are yet to be understood. Hence, intercluster reactions using these NCs can be studied to expand their chemistry. Reactions of NCs can be studied with other nanostructures and different bulk metals, which might give a new twist to the area.

Structures and properties: Over 100 multicomponent atomically precise alloy NCs comprising Au, Ag, Ni, Cu, Hg, Ir, Cd, Pd, and Pt have been synthesized till date using different synthesis methods. Most of these have been characterized with mass spectrometry, and about 50 have crystal structures. As a glaring gap, Fe and Co doping has not been accomplished yet in such clusters and these alloy clusters can be of potential interest due to their magnetic properties. Incorporation of lanthanides in NCs to make alloys will be an exciting study due to their interesting magnetic and photophysical properties. Even though Ni-doped NCs such as NiAu_{24} , NiAg_{24} , and NiAg_{28} have been synthesized, their magnetic properties have not been studied so far. These alloy NCs can show multiple phenomena such as circularly polarized luminescence, magneto-fluorescence, etc., which will help to broaden their applications.

Structures of multimetallic NCs will provide details of their optical and electronic properties. Unlike bimetallic NCs, the structure of tri- and tetrametallic NCs are yet to be studied extensively. Mainly, two kinds of alloy NCs are observed, (i) keeping the structure and composition the same, a specific number of foreign atoms are doped and (ii) the structure and compositions are different and the extent of doping depends on the molar ratio of the precursors used. In both the cases, it is crucial to get a single product either by controlling the synthesis method or by isolating the cluster of interest. The isolation of a specific isomer will be highly interesting, which can induce the possibility of crystallization.

Dynamics and mechanism: The exchange of metal atoms and the ligands between two different NCs manifest the dynamic nature of the outer staple motifs of NCs and protecting ligands. The investigation of this chemical event will be interesting. Also, a detailed study of the metal–ligand interface by theoretical calculations can reveal important information. In addition, a mechanistic study of the interactions between two NCs in the transition state is essential to have a deeper understanding of intercluster reactions. Although interaction of clusters leading to dimers have been observed in mass spectrometry, these species have not been trapped. Cluster reactions go through such an intermediate and several such intermediates have been identified. However, none of them have been seen. With the advancements in cryo-electron microscopy, it might be possible to observe such species in solution. If that becomes possible, it will lead to a new understanding of atom transfer processes, how chemical bonds are modified, etc. The existence of Borromean rings may be understood from such studies.

Bulk properties: The availability of larger crystals will enable the measurements of various physical properties of NC solids such as electrical conductivity, mechanical properties, etc., which can open a new paradigm in NC-based research. A systematic effort in the properties of clusters has to occur. The mechanical response of a few monometallic NC solids has been studied; however, this new field need to be explored using various multimetallic NC solids.

Assemblies and superstructures: Supramolecular assemblies of NCs with different nanoparticles or molecules and NC-based metal–organic frameworks are emerging materials as they can be used as functional building blocks to make hierarchical frameworks with improved properties. Although a few assemblies have been made using monometallic NCs, the area is yet to be expanded to multimetallic alloy NCs, which can bring in several unprecedented properties.

While many of these will be pursued in the coming years, there are inherent challenges in this system. The principal one is related to the dynamics of atoms in this length scale. That would mean that stabilizing the cluster systems in the solution and solid state for extended periods would involve the use of specific ligands, which do not allow atom transfer to occur. However, in some other contexts, these dynamics may be advantageous also. The extent of dynamics may be the reason for their use in catalysis. Whatever be the case, understanding such processes will require a great amount of computational effort. As the size of the systems increases, these efforts will become increasingly demanding.

AUTHOR INFORMATION

Corresponding Author

Thalappil Pradeep – Department of Chemistry, DST Unit of Nanoscience (DST UNS) and Thematic Unit of Excellence (TUE), Indian Institute of Technology Madras, Chennai 600036, India; orcid.org/0000-0003-3174-534X; Email: pradeep@iitm.ac.in

Author

Esma Khatun – Department of Chemistry, DST Unit of Nanoscience (DST UNS) and Thematic Unit of Excellence

(TUE), Indian Institute of Technology Madras, Chennai 600036, India

Complete contact information is available at:
<https://pubs.acs.org/10.1021/acsoomega.0c04832>

Notes

The authors declare no competing financial interest.

ACKNOWLEDGMENTS

We thank the Department of Science and Technology, Government of India for constantly supporting our research program on nanomaterials. E.K. thanks the Indian Institute of Technology Madras for research and doctoral fellowships.

REFERENCES

- (1) Acheson, L. A History of Metals. *Science* **1960**, *132*, 887–888.
- (2) Maddin, R. *The Beginning of the Use of Metals and Alloys*. The MIT Press, 1988.
- (3) Pradeep, T.; Anshup. Noble Metal Nanoparticles for Water Purification: A Critical Review. *Thin Solid Films* **2009**, *517*, 6441–6478.
- (4) Talapin, D. V.; Shevchenko, E. V. Introduction: Nanoparticle Chemistry. *Chem. Rev.* **2016**, *116*, 10343–10345.
- (5) Sajanalal, P. R.; Khatun, E.; Pradeep, T. *Gold Nanoparticles*; Kirk-Othmer Encyclopedia, 2019.
- (6) Haruta, M.; Editor; *Gold Nanotechnology: Fundamentals and Applications*; Shi Emu Shi Shuppan Co., Ltd. 2009.
- (7) *The British Museum*. www.thebritishmuseum.ac.uk.
- (8) Barber, D. J.; Freestone, I. C. An investigation of the origin of the Lycurgus Cup by analytical transmission electron spectroscopy. *Archaeometry* **1990**, *32*, 33–45.
- (9) Faraday, M. X. The Bakerian Lecture: -Experimental Relations of Gold (and Other Metals) to Light. *Philos. Trans. R. Soc. London* **1857**, *147*, 145–181.
- (10) Chakraborty, I.; Pradeep, T. Atomically Precise Clusters of Noble Metals: Emerging Link between Atoms and Nanoparticles. *Chem. Rev.* **2017**, *117*, 8208–8271.
- (11) Jin, R.; Zeng, C.; Zhou, M.; Chen, Y. Atomically Precise Colloidal Metal Nanoclusters and Nanoparticles: Fundamentals and Opportunities. *Chem. Rev.* **2016**, *116*, 10346–10413.
- (12) Ferrando, R.; Jellinek, J.; Johnston, R. L. Nanoalloys: From Theory to Applications of Alloy Clusters and Nanoparticles. *Chem. Rev.* **2008**, *108*, 845–910.
- (13) Wang, S.; Li, Q.; Kang, X.; Zhu, M. Customizing the Structure, Composition, and Properties of Alloy Nanoclusters by Metal Exchange. *Acc. Chem. Res.* **2018**, *51*, 2784–2792.
- (14) Hossain, S.; Niihori, Y.; Nair, L. V.; Kumar, B.; Kurashige, W.; Negishi, Y. Alloy Clusters: Precise Synthesis and Mixing Effects. *Acc. Chem. Res.* **2018**, *51*, 3114–3124.
- (15) McPartlin, M.; Mason, R.; Malatesta, L. Novel Cluster Complexes of Gold(0)–Gold(I). *J. Chem. Soc. D* **1969**, *7*, 334–334.
- (16) Boer, F. P.; Flynn, J. J.; Hecht, J. K. Crystal and Molecular Structure of Cis-1,2-Diacetonyl-1,2,3,3-Tetra-Chlorocyclopropane. *J. Chem. Soc. B* **1970**, *4021*, 381.
- (17) Teo, B. K.; Zhang, H.; Shi, X. Design, Synthesis, and Structure of the Largest Trimetallic Cluster, [(Ph₃P)₁₀Au₁₂Ag₁₂PtCl₇]Cl: The First Example of a Trimetallic Biicosahedral Supracluster and Its Implication for the Vertex-Sharing Polyicosahedral Growth of the Au/Ag/Pt Ternary Cluster. *J. Am. Chem. Soc.* **1993**, *115*, 8489–8490.
- (18) Teo, B. K.; Zhang, H.; Shi, X. Site Preference in Vertex-Sharing Polyicosahedral Supraclusters Containing Groups 10 and 11 Metals and Their Bonding Implications: Syntheses and Structures of the First Au-Ag-M (M = Pt, Ni) Biicosahedral Clusters [(Ph₃P)₁₀Au₁₂Ag₁₂-PtCl₇]Cl and [(Ph₃P)₁₀Au₁₂Ag₁₂NiCl₇](SbF₆). *Inorg. Chem.* **1994**, *33*, 4086–4097.
- (19) Teo, B. K.; Zhang, H.; Shi, X. Molecular Architecture of a Novel Vertex-Sharing Biicosahedral Cluster [(p-Tol₃P)₁₀Au₁₃Ag₁₂Br₈](PF₆)

Containing a Staggered-Staggered-Staggered Configuration for the 25-Atom Metal Framework. *Inorg. Chem.* **1990**, *29*, 2083–2091.

(20) Shichibu, Y.; Negishi, Y.; Tsukuda, T.; Teranishi, T. Large-Scale Synthesis of Thiolated Au₂₅ Clusters via Ligand Exchange Reactions of Phosphine-Stabilized Au₁₁ Clusters. *J. Am. Chem. Soc.* **2005**, *127*, 13464–13465.

(21) Whetten, R. L.; Khoury, J. T.; Alvarez, M. M.; Murthy, S.; Vezmar, I.; Wang, Z. L.; Stephens, P. W.; Cleveland, C. L.; Luedtke, W. D.; Landman, U. Nanocrystal Gold Molecules. *Adv. Mater.* **1996**, *8*, 428–433.

(22) Zhu, M.; Aikens, C. M.; Hollander, F. J.; Schatz, G. C.; Jin, R. Correlating the Crystal Structure of A Thiol-Protected Au₂₅ Cluster and Optical Properties. *J. Am. Chem. Soc.* **2008**, *130*, 5883–5885.

(23) Donkers, R. L.; Lee, D.; Murray, R. W. Synthesis and Isolation of the Molecule-like Cluster Au₃₈(PhCH₂CH₂S)₂₄. *Langmuir* **2004**, *20*, 1945–1952.

(24) Li, J.; Ma, H. Z.; Reid, G. E.; Edwards, A. J.; Hong, Y.; White, J. M.; Mulder, R. J.; O'Hair, R. A. J. Synthesis and X-Ray Crystallographic Characterisation of Frustum-Shaped Ligated [Cu₁₈H₁₆(DPPE)₆]²⁺ and [Cu₁₆H₁₄(DPPA)₆]²⁺ Nanoclusters and Studies on Their H₂ Evolution Reactions. *Chem. - Eur. J.* **2018**, *24*, 2070–2074.

(25) Cook, A. W.; Jones, Z. R.; Wu, G.; Scott, S. L.; Hayton, T. W. An Organometallic Cu₂₀ Nanocluster: Synthesis, Characterization, Immobilization on Silica, and “Click” Chemistry. *J. Am. Chem. Soc.* **2018**, *140*, 394–400.

(26) Nimmala, P. R.; Yoon, B.; Whetten, R. L.; Landman, U.; Dass, A. Au₆₇(SR)₃₅ Nanomolecules: Characteristic Size-Specific Optical, Electrochemical, Structural Properties and First-Principles Theoretical Analysis. *J. Phys. Chem. A* **2013**, *117*, 504–517.

(27) Nimmala, P. R.; Dass, A. Au₃₆(SPh)₂₃ Nanomolecules. *J. Am. Chem. Soc.* **2011**, *133*, 9175–9177.

(28) Sakthivel, N. A.; Theivendran, S.; Ganeshraj, V.; Oliver, A. G.; Dass, A. Crystal Structure of Faradaurate-279: Au₂₇₉(SPh^tBu)₈₄ Plasmonic Nanocrystal Molecules. *J. Am. Chem. Soc.* **2017**, *139*, 15450–15459.

(29) Joshi, C. P.; Bootharaju, M. S.; Alhilaly, M. J.; Bakr, O. M. [Ag₂₅(SR)₁₈]⁻: The “Golden” Silver Nanoparticle Silver Nanoparticle. *J. Am. Chem. Soc.* **2015**, *137*, 11578–11581.

(30) AbdulHalim, L. G.; Bootharaju, M. S.; Tang, Q.; Del Gobbo, S.; AbdulHalim, R. G.; Eddaoudi, M.; Jiang, D.; Bakr, O. M. Ag₂₉(BDT)₁₂(TPP)₄: A Tetravalent Nanocluster. *J. Am. Chem. Soc.* **2015**, *137*, 11970–11975.

(31) Yang, H.; Wang, Y.; Huang, H.; Gell, L.; Lehtovaara, L.; Malola, S.; Häkkinen, H.; Zheng, N. All-Thiol-Stabilized Ag₄₄ and Au₁₂Ag₃₂ Nanoparticles with Single-Crystal Structures. *Nat. Commun.* **2013**, *4*, 2422.

(32) Bootharaju, M. S.; Dey, R.; Gevers, L. E.; Hedhili, M. N.; Basset, J. M.; Bakr, O. M. A New Class of Atomically Precise, Hydride-Rich Silver Nanoclusters Co-Protected by Phosphines. *J. Am. Chem. Soc.* **2016**, *138*, 13770–13773.

(33) Nguyen, T. A. D.; Jones, Z. R.; Goldsmith, B. R.; Buratto, W. R.; Wu, G.; Scott, S. L.; Hayton, T. W. A Cu₂₅ Nanocluster with Partial Cu(0) Character. *J. Am. Chem. Soc.* **2015**, *137*, 13319–13324.

(34) Kang, X.; Wei, X.; Jin, S.; Yuan, Q.; Luan, X.; Pei, Y.; Wang, S.; Zhu, M.; Jin, R. Rational Construction of a Library of M₂₅ Nanoclusters from Monometallic to Tetrametallic. *Proc. Natl. Acad. Sci.* **2019**, *116*, 18834–18840.

(35) Soldan, G.; Aljuhani, M. A.; Bootharaju, M. S.; AbdulHalim, L. G.; Parida, M. R.; Emwas, A.-H.; Mohammed, O. F.; Bakr, O. M. Gold Doping of Silver Nanoclusters: A 26-Fold Enhancement in the Luminescence Quantum Yield. *Angew. Chem., Int. Ed.* **2016**, *55*, 5749–5753.

(36) Kumara, C.; Gagnon, K. J.; Dass, A. X-Ray Crystal Structure of Au_{38-x}Ag_x(SCH₂CH₂Ph)₂₄ Alloy Nanomolecules. *J. Phys. Chem. Lett.* **2015**, *6*, 1223–1228.

(37) Udayabhaskararao, T.; Sun, Y.; Goswami, N.; Pal, S. K.; Balasubramanian, K.; Pradeep, T. Ag₇Au₆: A 13-Atom Alloy Quantum Cluster. *Angew. Chem., Int. Ed.* **2012**, *51*, 2155–2159.

(38) Li, Q.; Wang, S.; Kirschbaum, K.; Lambright, K. J.; Das, A.; Jin, R. Heavily Doped Au_{25-x}Ag_x(SC₆H₁₁)₁₈⁻ Nanoclusters: Silver Goes from the Core to the Surface. *Chem. Commun.* **2016**, *52*, 5194–5197.

(39) Du, Y.; Guan, Z.-J.; Wen, Z.-R.; Lin, Y.-M.; Wang, Q.-M. Ligand-Controlled Doping Effects in Alloy Nanoclusters Au₄Ag₂₃ and Au₅Ag₂₄. *Chem. Eur. J.* **2018**, *24*, 16029–16035.

(40) Kang, X.; Xiong, L.; Wang, S.; Yu, H.; Jin, S.; Song, Y.; Chen, T.; Zheng, L.; Pan, C.; Pei, Y.; Zhu, M. Shape-Controlled Synthesis of Trimetallic Nanoclusters: Structure Elucidation and Properties Investigation. *Chem. Eur. J.* **2016**, *22*, 17145–17150.

(41) Yang, S.; Wang, S.; Jin, S.; Chen, S.; Sheng, H.; Zhu, M. A Metal Exchange Method for Thiolate-Protected Tri-Metal M₁Ag_xAu_{24-x}(SR)₁₈⁰ (M = Cd/Hg) Nanoclusters. *Nanoscale* **2015**, *7*, 10005–10007.

(42) Sharma, S.; Kurashige, W.; Nobusada, K.; Negishi, Y. Effect of Trimetalization in Thiolate-Protected Au_{24-n}Cu_nPd Clusters. *Nanoscale* **2015**, *7*, 10606–10612.

(43) Kimura, K.; Sugimoto, N.; Sato, S.; Yao, H.; Negishi, Y.; Tsukuda, T. Size Determination of Gold Clusters by Polyacrylamide Gel Electrophoresis in a Large Cluster Region. *J. Phys. Chem. C* **2009**, *113*, 14076–14082.

(44) Knoppe, S.; Boudon, J.; Dolamic, I.; Dass, A.; Bürgi, T. Size Exclusion Chromatography for Semipreparative Scale Separation of Au₃₈(SR)₂₄ and Au₄₀(SR)₂₄ and Larger Clusters. *Anal. Chem.* **2011**, *83*, 5056–5061.

(45) Negishi, Y.; Nobusada, K.; Tsukuda, T. Glutathione-Protected Gold Clusters Revisited: Bridging the Gap between Gold(I)–Thiolate Complexes and Thiolate-Protected Gold Nanocrystals. *J. Am. Chem. Soc.* **2005**, *127*, 5261–5270.

(46) Chen, T.; Yao, Q.; Nasaruddin, R. R.; Xie, J. Electrospray Ionization Mass Spectrometry: A Powerful Platform for Noble-Metal Nanocluster Analysis. *Angew. Chem., Int. Ed.* **2019**, *58*, 11967–11977.

(47) Heaven, M. W.; Dass, A.; White, P. S.; Holt, K. M.; Murray, R. W. Crystal Structure of the Gold Nanoparticle [N(C₈H₁₇)₄]-[Au₂₅(SCH₂CH₂Ph)₁₈]. *J. Am. Chem. Soc.* **2008**, *130*, 3754–3755.

(48) Kumara, C.; Aikens, C. M.; Dass, A. X-Ray Crystal Structure and Theoretical Analysis of Au_{25-x}Ag_x(SCH₂CH₂Ph)₁₈⁻ Alloy. *J. Phys. Chem. Lett.* **2014**, *5*, 461–466.

(49) Nannenga, B. L.; Gonen, T. MicroED: A Versatile CryoEM Method for Structure Determination. *Emerg. Top. Life Sci.* **2018**, *2*, 1–8.

(50) Roduner, E. Superatom Chemistry: Promising Properties of near-Spherical Noble Metal Clusters. *Phys. Chem. Chem. Phys.* **2018**, *20*, 23812–23826.

(51) Häkkinen, H. Atomic and Electronic Structure of Gold Clusters: Understanding Flakes, Cages and Superatoms from Simple Concepts. *Chem. Soc. Rev.* **2008**, *37*, 1847–1859.

(52) Bertorelle, F.; Russier-Antoine, I.; Calin, N.; Comby-Zerbino, C.; Bensalah-Ledoux, A.; Guy, S.; Dugourd, P.; Brevet, P.-F.; Sanader, Ž.; Krstić, M.; et al. Au₁₀(SG)₁₀: A Chiral Gold Catenane Nanocluster with Zero Confined Electrons. Optical Properties and First-Principles Theoretical Analysis. *J. Phys. Chem. Lett.* **2017**, *8*, 1979–1985.

(53) Weerawardene, K. L. D. M.; Häkkinen, H.; Aikens, C. M. Connections Between Theory and Experiment for Gold and Silver Nanoclusters. *Annu. Rev. Phys. Chem.* **2018**, *69*, 205–229.

(54) Wang, S.; Meng, X.; Das, A.; Li, T.; Song, Y.; Cao, T.; Zhu, X.; Zhu, M.; Jin, R. A 200-Fold Quantum Yield Boost in the Photoluminescence of Silver-Doped Ag_xAu_{25-x}Nanoclusters: The 13th Silver Atom Matters. *Angew. Chem., Int. Ed.* **2014**, *53*, 2376–2380.

(55) Suyama, M.; Takano, S.; Nakamura, T.; Tsukuda, T. Stoichiometric Formation of Open-Shell [PtAu₂₄(SC₂H₄Ph)₁₈]⁻ via Spontaneous Electron Proportionation between [PtAu₂₄(SC₂H₄Ph)₁₈]²⁻ and [PtAu₂₄(SC₂H₄Ph)₁₈]⁰. *J. Am. Chem. Soc.* **2019**, *141*, 14048–14051.

(56) Huifeng, Q.; Ellen, B.; Zhu, Y.; Jin, R. Doping 25-Atom and 38-Atom Gold Nanoclusters with Palladium. *Acta Phys.-Chim. Sin.* **2011**, *27*, 513–519.

(57) Fields-Zinna, C. A.; Crowe, M. C.; Dass, A.; Weaver, J. E. F.; Murray, R. W. Mass Spectrometry of Small Bimetal Monolayer-Protected Clusters. *Langmuir* **2009**, *25*, 7704–7710.

- (58) Kwak, K.; Choi, W.; Tang, Q.; Kim, M.; Lee, Y.; Jiang, D.-E.; Lee, D. A Molecule-like PtAu₂₄(SC₆H₁₃)₁₈ Nanocluster as an Electrocatalyst for Hydrogen Production. *Nat. Commun.* **2017**, *8*, 14723.
- (59) Xie, S.; Tsunoyama, H.; Kurashige, W.; Negishi, Y.; Tsukuda, T. Enhancement in Aerobic Alcohol Oxidation Catalysis of Au₂₅ Clusters by Single Pd Atom Doping. *ACS Catal.* **2012**, *2*, 1519–1523.
- (60) Yan, J.; Su, H.; Yang, H.; Malola, S.; Lin, S.; Häkkinen, H.; Zheng, N. Total Structure and Electronic Structure Analysis of Doped Thiolated Silver [MAg₂₄(SR)₁₈]²⁻ (M = Pd, Pt) Clusters. *J. Am. Chem. Soc.* **2015**, *137*, 11880–11883.
- (61) Jin, R.; Zhao, S.; Xing, Y.; Jin, R. All-Thiolate-Protected Silver and Silver-Rich Alloy Nanoclusters with Atomic Precision: Stable Sizes, Structural Characterization and Optical Properties. *CrystEngComm* **2016**, *18*, 3996–4005.
- (62) Liu, Y.; Chai, X.; Cai, X.; Chen, M.; Jin, R.; Ding, W.; Zhu, Y. Central Doping of a Foreign Atom into the Silver Cluster for Catalytic Conversion of CO₂ toward C–C Bond Formation. *Angew. Chem., Int. Ed.* **2018**, *57*, 9775–9779.
- (63) Kang, X.; Silalai, C.; Lv, Y.; Sun, G.; Chen, S.; Yu, H.; Xu, F.; Zhu, M. Au₁₅Ag₃(SPhMe₂)₁₄ Nanoclusters – Crystal Structure and Insights into Ligand-Induced Variation. *Eur. J. Inorg. Chem.* **2017**, *2017*, 1414–1419.
- (64) Molina, B.; Tlahuice-Flores, A. Thiolated Au₁₈ Cluster: Preferred Ag Sites for Doping, Structures, and Optical and Chiroptical Properties. *Phys. Chem. Chem. Phys.* **2016**, *18*, 1397–1403.
- (65) Jin, R.; Nobusada, K. Doping and Alloying in Atomically Precise Gold Nanoparticles. *Nano Res.* **2014**, *7*, 285–300.
- (66) Kang, X.; Li, Y.; Zhu, M.; Jin, R. Atomically Precise Alloy Nanoclusters: Syntheses, Structures, and Properties. *Chem. Soc. Rev.* **2020**, *49*, 6443–6514.
- (67) Kawawaki, T.; Imai, Y.; Suzuki, D.; Kato, S.; Kobayashi, I.; Suzuki, T.; Kaneko, R.; Hossain, S.; Negishi, Y. Atomically Precise Alloy Nanoclusters. *Chem. Eur. J.* **2020**, 16145.
- (68) Kang, X.; Zhu, M. Transformation of Atomically Precise Nanoclusters by Ligand-Exchange. *Chem. Mater.* **2019**, *31*, 9939–9969.
- (69) Higaki, T.; Li, Y.; Zhao, S.; Li, Q.; Li, S.; Du, X.-S.; Yang, S.; Chai, J.; Jin, R. Atomically Tailored Gold Nanoclusters for Catalytic Application. *Angew. Chem., Int. Ed.* **2019**, *58*, 8291–8302.
- (70) Kang, X.; Zhu, M. Tailoring the Photoluminescence of Atomically Precise Nanoclusters. *Chem. Soc. Rev.* **2019**, *48*, 2422–2457.
- (71) Teo, B. K.; Keating, K. Novel Tricosahedral Structure of the Largest Metal Alloy Cluster: hexachlorododecakis(triphenylphosphine)-gold-silver cluster [(Ph₃P)₁₂Au₁₃Ag₁₂Cl₆]^{M+}. *J. Am. Chem. Soc.* **1984**, *106*, 2224–2226.
- (72) Teo, B. K.; Shi, X.; Zhang, H. Cluster Rotamerism of a 25-Metal-Atom Cluster [(Ph₃P)₁₀Au₁₃Ag₁₂Br₈]⁺ Monocation: A Molecular Rotary Unit. *J. Chem. Soc., Chem. Commun.* **1992**, *17*, 1195.
- (73) Teo, B. K.; Zhang, H.; Shi, X. Cluster of Clusters: A Modular Approach to Large Metal Clusters. Structural Characterization of a 38-Atom Cluster [(p-Tol₃P)₁₂Au₁₈Ag₂₀Cl₁₄] Based on Vertex-Sharing Tricosahedra. *J. Am. Chem. Soc.* **1990**, *112*, 8552–8562.
- (74) Haggin, J. Illinois Scientists Synthesize Huge Cluster. *Chem. Eng. News Arch.* **1989**, *67*, 6.
- (75) Brust, M.; Walker, M.; Bethell, D.; Schiffrin, D. J.; Whyman, R. Synthesis of Thiol-Derivatized Gold Nanoparticles in a Two-Phase Liquid–Liquid System. *J. Chem. Soc., Chem. Commun.* **1994**, *0*, 801–802.
- (76) Kauffman, D. R.; Alfonso, D.; Matranga, C.; Qian, H.; Jin, R. A Quantum Alloy: The Ligand-Protected Au_{25-x}Ag_x(SR)₁₈ Cluster. *J. Phys. Chem. C* **2013**, *117*, 7914–7923.
- (77) Negishi, Y.; Munakata, K.; Ohgake, W.; Nobusada, K. Effect of Copper Doping on Electronic Structure, Geometric Structure, and Stability of Thiolate-Protected Au₂₅ Nanoclusters. *J. Phys. Chem. Lett.* **2012**, *3*, 2209–2214.
- (78) Negishi, Y.; Kurashige, W.; Niihori, Y.; Iwasa, T.; Nobusada, K. Isolation, Structure, and Stability of a Dodecanethiolate-Protected Pd₁Au₂₄ Cluster. *Phys. Chem. Chem. Phys.* **2010**, *12*, 6219–6225.
- (79) Negishi, Y.; Iwai, T.; Ide, M. Continuous Modulation of Electronic Structure of Stable Thiolate-Protected Au₂₅ Cluster by Ag Doping. *Chem. Commun.* **2010**, *46*, 4713–4715.
- (80) Biltek, S. R.; Mandal, S.; Sen, A.; Reber, A. C.; Pedicini, A. F.; Khanna, S. N. Synthesis and Structural Characterization of an Atom-Precise Bimetallic Nanocluster, Ag₄Ni₂(DMSA)₄. *J. Am. Chem. Soc.* **2013**, *135*, 20.
- (81) Deng, G.; Malola, S.; Yan, J.; Han, Y.; Yuan, P.; Zhao, C.; Yuan, X.; Lin, S.; Tang, Z.; Teo, B. K.; et al. From Symmetry Breaking to Unraveling the Origin of the Chirality of Ligated Au₁₃Cu₂ Nanoclusters. *Angew. Chem., Int. Ed.* **2018**, *57*, 3421–3425.
- (82) Dharmaratne, A. C.; Dass, A. Au_{144-x}Cu_x(SC₆H₁₃)₆₀ Nanomolecules: Effect of Cu Incorporation on Composition and Plasmon-like Peak Emergence in Optical Spectra. *Chem. Commun.* **2014**, *50*, 1722.
- (83) Jensen, K. M. Ø.; Juhas, P.; Tofanelli, M. A.; Heinecke, C. L.; Vaughan, G.; Ackerson, C. J.; Billinge, S. J. L. Polymorphism in Magic-Sized Au₁₄₄(SR)₆₀ Clusters. *Nat. Commun.* **2016**, *7*, 11859.
- (84) Zeng, J. L.; Guan, Z. J.; Du, Y.; Nan, Z. A.; Lin, Y. M.; Wang, Q. M. Chloride-Promoted Formation of a Bimetallic Nanocluster Au₃₀Ag₃₀ and the Total Structure Determination. *J. Am. Chem. Soc.* **2016**, *138*, 7848–7851.
- (85) Yan, J.; Su, H.; Yang, H.; Hu, C.; Malola, S.; Lin, S.; Teo, B. K.; Häkkinen, H.; Zheng, N. Asymmetric Synthesis of Chiral Bimetallic [Ag₂₈Cu₁₂(SR)₂₄]⁴⁻ Nanoclusters via Ion Pairing. *J. Am. Chem. Soc.* **2016**, *138*, 12751–12754.
- (86) Wang, S.; Jin, S.; Yang, S.; Chen, S.; Song, Y.; Zhang, J.; Zhu, M. Total Structure Determination of Surface Doping [Ag₄₆Au₂₄(SR)₃₂]- (BPh₄)₂ Nanocluster and Its Structure-Related Catalytic Property. *Sci. Adv.* **2015**, *1*, No. e1500441.
- (87) Conn, B. E.; Atnagulov, A.; Yoon, B.; Barnett, R. N.; Landman, U.; Bigioni, T. P. Confirmation of a de Novo Structure Prediction for an Atomically Precise Monolayer-Coated Silver Nanoparticle. *Sci. Adv.* **2016**, *2*, No. e1601609.
- (88) Kauffman, D. R.; Alfonso, D.; Matranga, C.; Qian, H.; Jin, R. A Quantum Alloy: The Ligand-Protected Au_{25-x}Ag_x(SR)₁₈ Cluster. *J. Phys. Chem. C* **2013**, *117*, 7914–7923.
- (89) Khatun, E.; Chakraborty, P.; Jacob, B. R.; Paramasivam, G.; Boduazzaman, M.; Dar, W. A.; Pradeep, T. Intercluster Reactions Resulting in Silver-Rich Trimetallic Nanoclusters. *Chem. Mater.* **2020**, *32*, 611–619.
- (90) Kanters, R. P. F.; Bour, J. J.; Schlebos, P. P. J.; Bosman, W. P.; Behm, H.; Steggerda, J. J.; Ito, L. N.; Pignolet, L. H. Structure and Properties of the Hydride-Containing Cluster Ion hydrido-(triphenylphosphine)heptakis[(triphenylphosphine)gold]platinum(2+). *Inorg. Chem.* **1989**, *28*, 2591–2594.
- (91) Wang, S.; Song, Y.; Jin, S.; Liu, X.; Zhang, J.; Pei, Y.; Meng, X.; Chen, M.; Li, P.; Zhu, M. Metal Exchange Method Using Au₂₅ Nanoclusters as Templates for Alloy Nanoclusters with Atomic Precision. *J. Am. Chem. Soc.* **2015**, *137*, 4018–4021.
- (92) Gan, Z.; Xia, N.; Wu, Z. Discovery, Mechanism, and Application of Antialgalvanic Reaction. *Acc. Chem. Res.* **2018**, *51*, 2774–2783.
- (93) Copley, R. C. B.; Mingos, D. M. P. Synthesis and Characterization of the Centred Icosahedral Cluster Series [Au₂MIB₄Cl₄(PMePh₂)₈][C₂B₉H₁₂], Where MIB = Au, Ag or Cu. *J. Chem. Soc. Dalton Trans.* **1996**, *4*, 491.
- (94) Li, Q.; Lambright, K. J.; Taylor, M. G.; Kirschbaum, K.; Luo, T. Y.; Zhao, J.; Mpourmpakis, G.; Mokashi-Punekar, S.; Rosi, N. L.; Jin, R. Reconstructing the Surface of Gold Nanoclusters by Cadmium Doping. *J. Am. Chem. Soc.* **2017**, *139*, 17779–17782.
- (95) Kang, X.; Xiong, L.; Wang, S.; Pei, Y.; Zhu, M. Combining the Single-Atom Engineering and Ligand-Exchange Strategies: Obtaining the Single-Heteroatom-Doped Au₁₆Ag₁(S-Adm)₁₃ Nanocluster with Atomically Precise Structure. *Inorg. Chem.* **2017**, *57*, 335–342.
- (96) Sharma, S.; Yamazoe, S.; Ono, T.; Kurashige, W.; Niihori, Y.; Nobusada, K.; Tsukuda, T.; Negishi, Y. Tuning the Electronic Structure of Thiolate-Protected 25-Atom Clusters by Co-Substitution with Metals Having Different Preferential Sites. *Dalton Trans.* **2016**, *45*, 18064–18068.

- (97) Kazan, R.; Zhang, B.; Bürgi, T. Au₃₈Cu₁(2-PET)₂₄ nanocluster: Synthesis, Enantioseparation and Luminescence. *Dalton Trans.* **2017**, 46, 7708–7713.
- (98) Biltek, S. R.; Sen, A.; Pedicini, A. F.; Reber, A. C.; Khanna, S. N. Isolation and Structural Characterization of a Silver–Platinum Nanocluster, Ag₄Pt₃(DMSA)₄. *J. Phys. Chem. A* **2014**, *118*, 8314–8319.
- (99) Liu, X.; Yuan, J.; Chen, J.; Yang, J.; Wu, Z. The Synthesis of Chiral Ag₄Pd₂(SR)₈ by Nonreplaced Galvanic Reaction. *Part. Part. Syst. Charact.* **2019**, *36*, 1900003.
- (100) Yang, H.; Wang, Y.; Lei, J.; Shi, L.; Wu, X.; Mäkinen, V.; Lin, S.; Tang, Z.; He, J.; Häkkinen, H.; et al. Ligand-Stabilized Au₁₃Cu_x (x = 2, 4, 8) Bimetallic Nanoclusters: Ligand Engineering to Control the Exposure of Metal Sites. *J. Am. Chem. Soc.* **2013**, *135*, 9568–9571.
- (101) Wang, Y.; Su, H.; Xu, C.; Li, G.; Gell, L.; Lin, S.; Tang, Z.; Häkkinen, H.; Zheng, N. An Intermetallic Au₂₄Ag₂₀ Superatom Nanocluster Stabilized by Labile Ligands. *J. Am. Chem. Soc.* **2015**, *137*, 4324–4327.
- (102) Tian, S.; Liao, L.; Yuan, J.; Yao, C.; Chen, J.; Yang, J.; Wu, Z. Structures and Magnetism of Mono-Palladium and Mono-Platinum Doped Au₂₅(PET)₁₈ Nanoclusters. *Chem. Commun.* **2016**, *52*, 9873–9876.
- (103) Negishi, Y.; Igarashi, K.; Munakata, K.; Ohgake, W.; Nobusada, K. Palladium Doping of Magic Gold Cluster Au₃₈(SC₂H₄Ph)₂₄: Formation of Pd₂Au₃₆(SC₂H₄Ph)₂₄ with Higher Stability than Au₃₈(SC₂H₄Ph)₂₄. *Chem. Commun.* **2012**, *48*, 660–662.
- (104) Teo, B. K.; Dang, H.; Campana, C. F.; Zhang, H. Synthesis, Structure, and Characterization of (MePh₂P)₁₀Au₁₂Ag₁₃Br₉: The First Example of a Neutral Bi-Icosahedral Au Ag Cluster with a Novel Seven-Membered Satellite Ring of Bridging Ligands. *Polyhedron* **1998**, *17*, 617–621.
- (105) Lin, Y.-R.; Kishore, P. V. V. N.; Liao, J.-H.; Kahlal, S.; Liu, Y.-C.; Chiang, M.-H.; Saillard, J.-Y.; Liu, C. W. Synthesis, Structural Characterization and Transformation of an Eight-Electron Superatomic Alloy, [Au@Ag₁₉{S₂P(OPr)₂}]₁₂. *Nanoscale* **2018**, *10*, 6855–6860.
- (106) Li, Y.; Zhou, M.; Jin, S.; Xiong, L.; Yuan, Q.; Du, W.; Pei, Y.; Wang, S.; Zhu, M. Total Structural Determination of [Au₁Ag₂₄(Dppm)₃(SR)₁₇]²⁺ Comprising an Open Icosahedral Au₁Ag₁₂ Core with Six Free Valence Electrons. *Chem. Commun.* **2019**, *55*, 6457–6460.
- (107) Bootharaju, M. S.; Kozlov, S. M.; Cao, Z.; Harb, M.; Maity, N.; Shkurenko, A.; Parida, M. R.; Hedhili, M. N.; Eddaoudi, M.; Mohammed, O. F.; et al. Doping-Induced Anisotropic Self-Assembly of Silver Icosahedra in [Pt₂Ag₂₃Cl₂(PPh₃)₁₀] Nanoclusters. *J. Am. Chem. Soc.* **2017**, *139*, 1053–1056.
- (108) He, L.; Yuan, J.; Xia, N.; Liao, L.; Liu, X.; Gan, Z.; Wang, C.; Yang, J.; Wu, Z. Kernel Tuning and Nonuniform Influence on Optical and Electrochemical Gaps of Bimetal Nanoclusters. *J. Am. Chem. Soc.* **2018**, *140*, 3487–3490.
- (109) Kang, X.; Li, X.; Yu, H.; Lv, Y.; Sun, G.; Li, Y.; Wang, S.; Zhu, M. Modulating Photo-Luminescence of Au₂Cu₆ Nanoclusters: Via Ligand-Engineering. *RSC Adv.* **2017**, *7*, 28606–28609.
- (110) Jin, S.; Liu, W.; Hu, D.; Zou, X.; Kang, X.; Du, W.; Chen, S.; Wei, S.; Wang, S.; Zhu, M. Aggregation-Induced Emission (AIE) in Ag–Au Bimetallic Nanocluster. *Chem. Eur. J.* **2018**, *24*, 3712–3715.
- (111) Liu, C.; Ren, X.; Lin, F.; Fu, X.; Lin, X.; Li, T.; Sun, K.; Huang, J. Structure of the Au_{23–x}Ag_x(S-Adm)₁₅ Nanocluster and Its Application for Photocatalytic Degradation of Organic Pollutants. *Angew. Chem., Int. Ed.* **2019**, *58*, 11335–11339.
- (112) Zou, X.; Li, Y.; Jin, S.; Kang, X.; Wei, X.; Wang, S.; Meng, X.; Zhu, M. Doping Copper Atoms into the Nanocluster Kernel: Total Structure Determination of [Cu₃₀Ag₆₁(SAdm)₃₈S₃](BPh₄). *J. Phys. Chem. Lett.* **2020**, *11*, 2272–2276.
- (113) Zhou, M.; Jin, S.; Wei, X.; Yuan, Q.; Wang, S.; Du, Y.; Zhu, M. Reversible Cu–S Motif Transformation and Au₄ Distortion via Thiol Ligand Exchange Engineering. *J. Phys. Chem. C* **2020**, *124*, 7531–7538.
- (114) Jin, S.; Zhou, M.; Kang, X.; Li, X.; Du, W.; Wei, X.; Chen, S.; Wang, S.; Zhu, M. Three-dimensional Octameric Assembly of Icosahedral M₁₃ Units in [Au₈Ag₅₇(Dppp)₄(C₆H₁₁S)₃₂Cl₂]Cl and Its [Au₈Ag₅₅(Dppp)₄(C₆H₁₁S)₃₄](BPh₄)₂ Derivative. *Angew. Chem.* **2020**, *132*, 3919–3923.
- (115) Sun, W.; Jin, S.; Du, W.; Kang, X.; Chen, A.; Wang, S.; Sheng, H.; Zhu, M. Total Structure Determination of the Pt₁Ag₉[P(Ph-F)₃]₇Cl₃Nanocluster. *Eur. J. Inorg. Chem.* **2020**, *2020*, 590–594.
- (116) Higaki, T.; Liu, C.; Morris, D. J.; He, G.; Luo, T. Y.; Sfeir, M. Y.; Zhang, P.; Rosi, N. L.; Jin, R. Au_{130–x}Ag_x Nanoclusters with Non-Metallicity: A Drum of Silver-Rich Sites Enclosed in a Marks-Decahedral Cage of Gold-Rich Sites. *Angew. Chem., Int. Ed.* **2019**, *58*, 18798–18802.
- (117) Kang, X.; Abroshan, H.; Wang, S.; Zhu, M. Free Valence Electron Centralization Strategy for Preparing Ultrastable Nanoclusters and Their Catalytic Application. *Inorg. Chem.* **2019**, *58*, 11000–11009.
- (118) Wen, Z.-R.; Guan, Z.-J.; Zhang, Y.; Lin, Y.-M.; Wang, Q.-M. [Au₇Ag₉(Dppf)₃(CF₃CO₂)₇BF₄]_n: A Linear Nanocluster Polymer from Molecular Au–Ag₈ Clusters Covalently Linked by Silver Atoms. *Chem. Commun.* **2019**, *55*, 12992–12995.
- (119) Zou, X.; Jin, S.; Wang, S.; Zhu, M.; Jin, R. Tailoring the Structure of 32-Metal-Atom Nanoclusters by Ligands and Alloying. *Nano Futures* **2018**, *2*, No. 045004.
- (120) Jin, S.; Xu, F.; Du, W.; Kang, X.; Chen, S.; Zhang, J.; Li, X.; Hu, D.; Wang, S.; Zhu, M. Isomerism in Au–Ag Alloy Nanoclusters: Structure Determination and Enantioseparation of [Au₉Ag₁₂(SR)₄(Dppm)₆X₆]³⁺. *Inorg. Chem.* **2018**, *57*, 5114–5119.
- (121) Bour, J. J.; Kanters, R. P. F.; Schlebos, P. P. J.; Bosman, W. P.; Behm, H.; Beurskens, P. T.; Steggerda, J. J. Hetero-Metallic Clusters. Synthesis and Characterization of [PtAu₈(PPh₃)₈](NO₃)₂ and [HPtAu₇(PPh₃)₈](NO₃)₂. *Recl. des Trav. Chim. des Pays-Bas* **1987**, *106*, 157–158.
- (122) Yang, H.; Wang, Y.; Yan, J.; Chen, X.; Zhang, X.; Häkkinen, H.; Zheng, N. Structural Evolution of Atomically Precise Thiolated Bimetallic [Au_{12+n}Cu₃₂(SR)_{30+n}]⁴⁺ (n = 0, 2, 4, 6) Nanoclusters. *J. Am. Chem. Soc.* **2014**, *136*, 7197–7200.
- (123) Yang, S.; Chen, S.; Xiong, L.; Liu, C.; Yu, H.; Wang, S.; Rosi, N. L.; Pei, Y.; Zhu, M. Total Structure Determination of Au₁₆(S-Adm)₁₂ and Cd₁Au₁₄(S^tBu)₁₂ and Implications for the Structure of Au₁₅(SR)₁₃. *J. Am. Chem. Soc.* **2018**, *140*, 10988–10994.
- (124) Qin, Z.; Zhao, D.; Zhao, L.; Xiao, Q.; Wu, T.; Zhang, J.; Wan, C.; Li, G. Tailoring the Stability, Photocatalysis and Photoluminescence Properties of Engineering. *Nanoscale Adv.* **2019**, *1*, 2529–2536.
- (125) Theivendran, S.; Chang, L.; Mukherjee, A.; Sementa, L.; Stener, M.; Fortunelli, A.; Dass, A. Principles of Optical Spectroscopy of Aromatic Alloy Nanomolecules: Au_{36–x}Ag_x(SPh^tBu)₂₄. *J. Phys. Chem. C* **2018**, *122*, 4524–4531.
- (126) Chai, J.; Lv, Y.; Yang, S.; Song, Y.; Zan, X.; Li, Q.; Yu, H.; Wu, M.; Zhu, M. X-Ray Crystal Structure and Optical Properties of Au_{38–x}Cu_x(2,4-(CH₃)₂C₆H₃S)₂₄ (x = 0–6) Alloy Nanocluster. *J. Phys. Chem. C* **2017**, *121*, 21665–21669.
- (127) Wan, X.-K.; Cheng, X.-L.; Tang, Q.; Han, Y.-Z.; Hu, G.; Jiang, D.-E.; Wang, Q.-M. Atomically Precise Bimetallic Au₁₉Cu₃₀ Nanocluster with an Icosidodecahedral Cu₃₀ Shell and an Alkynyl–Cu Interface. *J. Am. Chem. Soc.* **2017**, *139*, 9451–9454.
- (128) Wang, Z.; Senanayake, R.; Aikens, C. M.; Chen, W.-M.; Tung, C.-H.; Sun, D. Gold-Doped Silver Nanocluster [Au₃Ag₃₈(SCH₂Ph)₂₄X₅]^{2–} (X = Cl or Br). *Nanoscale* **2016**, *8*, 18905.
- (129) Hossain, S.; Imai, Y.; Motohashi, Y.; Chen, Z.; Suzuki, D.; Suzuki, T.; Kataoka, Y.; Hirata, M.; Ono, T.; Kurashige, W.; et al. Understanding and Designing One-Dimensional Assemblies of Ligand-Protected Metal Nanoclusters. *Mater. Horiz.* **2020**, *7*, 796.
- (130) Chen, J.; Liu, L.; Liu, X.; Liao, L.; Zhuang, S.; Zhou, S.; Yang, J.; Wu, Z. Gold-Doping of Double-Crown Pd Nanoclusters. *Chem. Eur. J.* **2017**, *23*, 18187–18192.
- (131) Chai, J.; Yang, S.; Lv, Y.; Chong, H.; Yu, H.; Zhu, M. Exposing the Delocalized Cu–S π Bonds on the Au₂₄Cu₆(SPh^tBu)₂₂ Nanocluster and Its Application in Ring-Opening Reactions. *Angew. Chem., Int. Ed.* **2019**, *58*, 15671–15674.
- (132) Rao, B.; Zhao, T.; Yang, S.; Chai, J.; Pan, Y.; Weng, S.; Yu, H.; Li, X.; Zhu, M. X-Ray Crystal Structure and Doping Mechanism of

Bimetallic Nanocluster $\text{Au}_{36-x}\text{Cu}_x(\text{m-MBT})_{24}$ ($x = 1-3$). *Dalton Trans.* **2018**, *47*, 475–480.

(133) Krishnadas, K. R.; Baksi, A.; Ghosh, A.; Natarajan, G.; Pradeep, T. Manifestation of Geometric and Electronic Shell Structures of Metal Clusters in Intercluster Reactions. *ACS Nano* **2017**, *11*, 6015–6023.

(134) Yang, S.; Chai, J.; Song, Y.; Fan, J.; Chen, T.; Wang, S.; Yu, H.; Li, X.; Zhu, M. In Situ Two-Phase Ligand Exchange: A New Method for the Synthesis of Alloy Nanoclusters with Precise Atomic Structures. *J. Am. Chem. Soc.* **2017**, *139*, 5668–5671.

(135) Choi, J.-P.; Fields-Zinna, C. A.; Stiles, R. L.; Balasubramanian, R.; Douglas, A. D.; Crowe, M. C.; Murray, R. W. Reactivity of $[\text{Au}_{25}(\text{SCH}_2\text{CH}_2\text{Ph})_{18}]^{1-}$ Nanoparticles with Metal Ions. *J. Phys. Chem. C* **2010**, *114*, 15890–15896.

(136) Wu, Z. Anti-Galvanic Reduction of Thiolate-Protected Gold and Silver Nanoparticles. *Angew. Chem., Int. Ed.* **2012**, *51*, 2934–2938.

(137) Bootharaju, M. S.; Joshi, C. P.; Parida, M. R.; Mohammed, O. F.; Bakr, O. M. Templated Atom-Precise Galvanic Synthesis and Structure Elucidation of a $[\text{Ag}_{24}\text{Au}(\text{SR})_{18}]^{-}$ Nanocluster. *Angew. Chem., Int. Ed.* **2016**, *55*, 824.

(138) Krishnadas, K. R.; Ghosh, A.; Baksi, A.; Chakraborty, I.; Natarajan, G.; Pradeep, T. Intercluster Reactions between $\text{Au}_{25}(\text{SR})_{18}$ and $\text{Ag}_{44}(\text{SR})_{30}$. *J. Am. Chem. Soc.* **2016**, *138*, 140–148.

(139) Du, W.; Jin, S.; Xiong, L.; Chen, M.; Zhang, J.; Zou, X.; Pei, Y.; Wang, S.; Zhu, M. $\text{Ag}_{50}(\text{Dppm})_6(\text{SR})_{30}$ and Its Homologue $\text{Au}_{50-x}(\text{Dppm})_6(\text{SR})_{30}$ Alloy Nanocluster: Seeded Growth, Structure Determination, and Differences in Properties. *J. Am. Chem. Soc.* **2017**, *139*, 1618–1624.

(140) Zheng, K.; Fung, V.; Yuan, X.; Jiang, D. E.; Xie, J. Real Time Monitoring of the Dynamic Intracluster Diffusion of Single Gold Atoms into Silver Nanoclusters. *J. Am. Chem. Soc.* **2019**, *141*, 18977–18983.

(141) He, L.; Gan, Z.; Xia, N.; Liao, L.; Wu, Z. Alternating Array Stacking of Ag_{26}Au and Ag_{24}Au Nanoclusters. *Angew. Chem.* **2019**, *131*, 10002–10006.

(142) Bhat, S.; Baksi, A.; Mudedla, S. K.; Natarajan, G.; Subramanian, V.; Pradeep, T. $\text{Au}_{22}\text{Ir}_3(\text{PET})_{18}$: An Unusual Alloy Cluster through Intercluster Reaction. *J. Phys. Chem. Lett.* **2017**, *8*, 2787–2793.

(143) Xia, N.; Wu, Z. Doping Au_{25} Nanoparticles Using Ultrasmall Silver or Copper Nanoparticles as the Metal Source. *J. Mater. Chem. C* **2016**, *4*, 4125–4128.

(144) Ghosh, A.; Ghosh, D.; Khatun, E.; Chakraborty, P.; Pradeep, T. Unusual Reactivity of Dithiol Protected Clusters in Comparison to Monothiol Protected Clusters: Studies Using $\text{Ag}_{51}(\text{BDT})_{19}(\text{TPP})_3$ and $\text{Ag}_{29}(\text{BDT})_{12}(\text{TPP})_4$. *Nanoscale* **2017**, *9*, 1068–1077.

(145) Bootharaju, M. S.; Kozlov, S. M.; Cao, Z.; Harb, M.; Parida, M. R.; Hedhili, M. N.; Mohammed, O. F.; Bakr, O. M.; Cavallo, L.; Basset, J.-M. Direct versus Ligand-Exchange Synthesis of $[\text{PtAg}_{28}(\text{BDT})_{12}(\text{TPP})_4]^{4-}$ Nanoclusters: Effect of a Single-Atom Dopant on the Optoelectronic and Chemical Properties. *Nanoscale* **2017**, *9*, 9529–9536.

(146) Bootharaju, M. S.; Kozlov, S. M.; Cao, Z.; Shkurenko, A.; El-Zohry, A. M.; Mohammed, O. F.; Eddaoudi, M.; Bakr, O. M.; Cavallo, L.; Basset, J.-M. Tailoring the Crystal Structure of Nanoclusters Unveiled High Photoluminescence via Ion Pairing. *Chem. Mater.* **2018**, *30*, 2719–2725.

(147) Kang, X.; Xiong, L.; Wang, S.; Pei, Y.; Zhu, M. De-Assembly of Assembled $\text{Pt}_1\text{Ag}_{12}$ Units: Tailoring the Photoluminescence of Atomically Precise Nanoclusters. *Chem. Commun.* **2017**, *53*, 12564–12567.

(148) Kang, X.; Zhou, M.; Wang, S.; Jin, S.; Sun, G.; Zhu, M.; Jin, R. The Tetrahedral Structure and Luminescence Properties of Bi-Metallic $\text{Pt}_1\text{Ag}_{28}(\text{SR})_{18}(\text{PPh}_3)_4$ Nanocluster. *Chem. Sci.* **2017**, *8*, 2581–2587.

(149) Chen, S.; Du, W.; Qin, C.; Liu, D.; Tang, L.; Liu, Y.; Wang, S.; Zhu, M. Assembly of the Thiolated $[\text{Au}_1\text{Ag}_{22}(\text{S-Adm})_{12}]^{3+}$ Superatom Complex into a Framework Material through Direct Linkage by SbF_6^- Anions. *Angew. Chem., Int. Ed.* **2020**, *59*, 7542–7547.

(150) Li, Q.; Taylor, M. G.; Kirschbaum, K.; Lambright, K. J.; Zhu, X.; Mpourmpakis, G.; Jin, R. Site-Selective Substitution of Gold Atoms in the $\text{Au}_{24}(\text{SR})_{20}$ Nanocluster by Silver. *J. Colloid Interface Sci.* **2017**, *505*, 1202–1207.

(151) Kang, X.; Huang, L.; Liu, W.; Xiong, L.; Pei, Y.; Sun, Z.; Wang, S.; Wei, S.; Zhu, M. Reversible Nanocluster Structure Transformation between Face-Centered Cubic and Icosahedral Isomers. *Chem. Sci.* **2019**, *10*, 8685–8693.

(152) Li, Y.; Chen, M.; Wang, S.; Zhu, M. Intramolecular Metal Exchange Reaction Promoted by Thiol Ligands. *Nanomaterials* **2018**, *8*, 1070.

(153) Wang, S.; Abroshan, H.; Liu, C.; Luo, T.-Y.; Zhu, M.; Kim, H. J.; Rosi, N. L.; Jin, R. Shuttling Single Metal Atom into and out of a Metal Nanoparticle. *Nat. Commun.* **2017**, *8*, 848.

(154) Li, Q.; Luo, T.-Y.; Taylor, M. G.; Wang, S.; Zhu, X.; Song, Y.; Mpourmpakis, G.; Rosi, N. L.; Jin, R. Molecular “Surgery” on a 23-Gold-Atom Nanoparticle. *Sci. Adv.* **2017**, *3*, No. e1603193.

(155) Zeng, C.; Chen, Y.; Das, A.; Jin, R. Transformation Chemistry of Gold Nanoclusters: From One Stable Size to Another. *J. Phys. Chem. Lett.* **2015**, *6*, 2976–2986.

(156) Krishnadas, K. R.; Baksi, A.; Ghosh, A.; Natarajan, G.; Pradeep, T. Structure-Conserving Spontaneous Transformations between Nanoparticles. *Nat. Commun.* **2016**, *7*, 13447.

(157) Natarajan, G.; Mathew, A.; Negishi, Y.; Whetten, R. L.; Pradeep, T. A Unified Framework for Understanding the Structure and Modifications of Atomically Precise Monolayer Protected Gold Clusters. *J. Phys. Chem. C* **2015**, *119*, 27768–27785.

(158) Bose, P.; Chakraborty, P.; Mohanty, J. S.; Nonappa; Chowdhuri, A. R.; Khatun, E.; Ahuja, T.; Mahendranath, A.; Pradeep, T. Atom transfer between precision nanoclusters and polydispersed nanoparticles: a facile route for monodisperse alloy nanoparticles and their superstructures. *Nanoscale* **2020**, *12*, 22116–22128.

(159) Kazan, R.; Müller, U.; Bürgi, T. Doping of Thiolate Protected Gold Clusters through Reaction with Metal Surfaces. *Nanoscale* **2019**, *11*, 2938–2945.

(160) Krishnadas, K. R.; Natarajan, G.; Baksi, A.; Ghosh, A.; Khatun, E.; Pradeep, T. Metal–Ligand Interface in the Chemical Reactions of Ligand-Protected Noble Metal Clusters. *Langmuir* **2019**, *35*, 11243–11254.